論文 / 著書情報
Article / Book Information

Title	Divergent humidity-driven growth in urban air-conditioning energy demand under climate change
Authors	Xinchang ‘Cathy’ Li, Lei Zhao, Zhiwen Luo, Keith Oleson, Yifan Cheng, Xiaoxiong Xie, Alvin C. G. Varquez, Mitsuna Sekiya
Citation	Nature Cities
Pub. date	2026, 7
DOI	https://doi.org/10.1038/s44284-026-00474-4
Creative Commons	Information is in the article.

nature cities

Article https://doi.org/10.1038/s44284-026-00474-4

Divergent humidity-driven growth in urban air-conditioning energy demand under climate change

Received: 9 December 2025

Accepted: 17 June 2026

Published online: 24 July 2026

Check for updates

Xinchang 'Cathy' Li[1,2], Lei Zhao[1,3,4,5], Zhiwen Luo[6], Keith Oleson[7], Yifan Cheng[1], Xiaoxiong Xie[8], Alvin C. G. Varquez[9] & Mitsuna Sekiya[9]

Rapid urbanization and climate change are intensifying humid heat in cities, making air conditioning (AC) increasingly essential for both cooling and dehumidification. However, the evolving and spatially varied contribution of humidity to urban AC energy demand remains poorly understood, posing risks to climate-sensitive urban energy planning and building thermal design. Here, by coupling an updated urban building energy model with a global Earth system model, we project that urban dehumidification energy demand will rise by 47% globally under a high-emission scenario. Its contribution to total urban AC demand diverges markedly across regions owing to interacting changes in temperature and humidity that reshape city-specific building thermal design conditions. We further show that humidity amplifies the temperature sensitivity of urban AC demand across climate zones, leading to AC energy demand two to three times higher on humid days. These findings highlight the critical need to incorporate humidity dynamics into urban energy and infrastructure planning, particularly in rapidly urbanizing regions of the global south.

Humid heat is a growing concern in cities around the world[1–5]. To maintain indoor comfort and health, air conditioning (AC) has become increasingly important as an active adaptation strategy, providing both cooling (temperature reduction) and dehumidification[6]. Urban AC energy demand is thus projected to increase substantially under climate change and socioeconomic development[7–9]. This challenges cities' electricity infrastructure to be prepared for the growing demand and new buildings to be designed for a changing climate[10,11]. Such challenges are amplified for cities in the global south, as the majority are located in hot and humid climates and projected to experience substantial economic growth and rapid urbanization. This will necessitate the design and construction of urban buildings and energy infrastructures that can withstand the intensifying humid heat[10,12].

Humidity's contribution to building energy demand has been recognized, especially in wet climates[13–22]. However, its relative importance is still an open question. Substantial uncertainty and discrepancy exist in the current literature: local-scale studies report energy demand differences ranging from a few percent to more than 96% in different moisture conditions[16–22] (Extended Data Table 1), due to differences in study location, scope, methods, data and building type. This almost precludes drawing a consensus or conducting comparative analyses. Furthermore, the humidity effects will probably be altered or amplified

[1]Department of Civil and Environmental Engineering, The Grainger College of Engineering, University of Illinois Urbana-Champaign, Urbana, IL, USA. [2]Pacific Northwest National Laboratory, Richland, WA, USA. [3]National Center for Supercomputing Applications, University of Illinois Urbana-Champaign, Urbana, IL, USA. [4]Institute for Sustainability, Energy, and Environment, University of Illinois Urbana-Champaign, Urbana, IL, USA. [5]Department of Climate, Meteorology and Atmospheric Sciences, University of Illinois Urbana-Champaign, Urbana, IL, USA. [6]Welsh School of Architecture, Cardiff University, Cardiff, UK. [7]Climate and Global Dynamics Laboratory, NSF National Center for Atmospheric Research, Boulder, CO, USA. [8]School of Art, Design and Architecture, University of Plymouth, Plymouth, UK. [9]Department of Transdisciplinary Science and Engineering, Institute of Science Tokyo, Tokyo, Japan. e-mail: xinchang.li@pnnl.gov; leizhao@illinois.edu

https://doi.org/10.1038/s44284-026-00474-4

in the future, as climate change not only increases air temperature but also specific humidity[23–25]. This is because (1) increase in air temperature promotes evaporation of water from the surface, and (2) a warmer atmosphere has the capacity to hold more water vapor[24,25], so the extra water being evaporated can remain water vapor in the air. Heterogeneous surface warming and water availability lead to locally varied changes in temperature and humidity: while some cities with sufficient water availability may become warmer and more humid, other more water-limited cities may become warmer and drier[23]. These diverging changes will drive disparate AC energy demand responses that are crucial to understand over large spatiotemporal scales for the climate preparedness of our energy infrastructure and built environment.

Despite its critical importance, the evolving, spatially varied humidity effect remains largely excluded in large-scale energy demand projections used for long-term energy planning, which are predominantly made based on extrapolations from historical data. This is problematic for two reasons. First, the models for these projections often describe only the temperature dependency of energy use, without accounting for the humidity effect. They tend to use dry-bulb temperature[26–29] or other purely temperature-dependent metrics, such as heating and cooling degree days[23,30–32] as the only climatic predictors. Although the humidity effect is implicitly captured in the energy–temperature relationship, the heterogeneous changes in temperature and humidity induced by climate change means the humidity effect in such a relationship will evolve in the future, invalidating extrapolations. Second, these projections ignore the positive biophysical feedbacks between AC energy use and urban climate[7], where an increase in AC energy use will raise outdoor urban temperature and cause an additional increase to AC energy demand[33–37]. These city-scale feedbacks will accelerate under climate change, further modifying the energy–climate relationships distilled from historical data[7]. As a result, extrapolations, spatially or temporally, from current energy and climate relationships will lead to erroneous future projections that misrepresent the changing humidity or feedback dynamics. This severely harms our ability to provide reliable and actionable projections for urban energy planning.

These challenges are likely to be exacerbated during extreme days under climate change. Buildings and their systems are designed per building codes, standards and regulations, which typically base their requirements on past climate, with climate data representing average (Typical Meteorological Years[38]) or extreme (design conditions)[39] weather conditions of the past. As climate change makes extreme events longer, more frequent and more intense[23], buildings designed for a historical climate will suffer from higher rates of undesirable indoor conditions[40] and increased likelihood for demand spikes that are detrimental to power grids[10,38]. This poses risks for long-term energy infrastructure planning as well as short-term load balancing under intensifying urban humid heat. Thus, to systematically understand humidity-driven demand changes under climate change and future extremes in global cities, we need to dynamically simulate urban climate and building energy interactions with physics-based modeling in a globally coherent manner.

To this end, we develop a new physics-based parameterization scheme in this study to model indoor humidity and dehumidification energy demand in the urban building energy model (BEM) of the Community Earth System Model (CESM). The scheme adopts a setpoint approach and simulates both the sensible (for cooling) and latent (for dehumidification) AC energy demand required to maintain indoor comfort and health (Methods). The use of CESM and the updated urban BEM allows us to model cities' humidity-driven demand changes under climate change and future extremes in a globally coherent manner (Supplementary Note 1). We validate the scheme both on its ability to simulate total AC energy demand globally and on its performance simulating the relative contribution of sensible and latent heat load at the local scale (Methods). We conduct a global land-only simulation driven by atmospheric forcings from a fully-coupled simulation under a high-emission scenario, keeping socioeconomic factors such as AC adoption rate[41] and urban extent at the present-day level to isolate climate change effects (Methods). Daily average values of urban air temperature (T_u), relative humidity (RH), specific humidity (q) and sensible and latent heat load fluxes of urban AC energy demand (Q_c) for the first decade (2015–2024) and the last decade (2090–2099) of the simulation period are analyzed.

Increasing and diverging role of latent heat load under climate change

Globally, average urban dehumidification energy flux, represented by latent heat load flux, contributes 0.15 W m^{-2} to total urban AC energy flux between 2015 and 2024 in summer (Fig. 1a). This is 16% of the global average urban cooling energy (sensible heat load) flux, at 0.95 W m^{-2}. Cities with high latent heat load fluxes are concentrated near warm and humid coastal regions with high AC adoption rates (Extended Data Fig. 1), such as along the East coast of the contiguous USA, Eastern China, Japan and Thailand (see Supplementary Note 2 for a detailed analysis using Japanese cities as an illustrative example). By the end of the century, global average urban dehumidification energy flux increases by 47% to 0.22 W m^{-2} (Fig. 1b) under the high-emission scenario. This is a slightly larger increase in percentage compared with that of the sensible heat load flux, which increases by 44% to 1.69 W m^{-2}. All current hotspot regions experience an increase in latent heat load flux by 0.2–1 W m^{-2} (Fig. 1c). In addition, new hotspot regions emerge, such as eastern South America and western Indian Peninsula (Fig. 1b), despite their low present-day AC adoption rate (16% for Brazil and 5% for India, Extended Data Fig. 1), signifying strong urban humidification under climate change in these regions. This is consistent with urban humid heat projections in the literature[2], and alludes to the potential impact of high humid heat on the energy systems.

The relative contribution of latent heat load, represented by latent heat load fraction (Methods), displays a vastly different spatial pattern (Fig. 1d,e). Latent heat load fraction is calculated as latent heat load divided by total AC energy demand (the sum of latent and sensible heat load) and expressed in percentage form. It represents the relative importance of dehumidification in AC energy use. This metric is independent of AC adoption rate (Methods) and therefore provides insights that are applicable under changing AC adoption levels. Global average latent heat load fraction is 14% in 2015–2024 and decreases slightly to 13% in 2090–2099. Dehumidification takes up a relatively small fraction (less than 8%) of total AC energy demand in mid-to-high latitude regions in the Northern Hemisphere (30–90° N) where most of the developed nations reside. However, dehumidification dominates AC energy demand (latent heat load fraction up to 94%) for hot and humid urban areas located between 30° N and 30° S where developing nations are concentrated, such as Southeast Asia and equatorial regions of South America and Africa (Fig. 1d,e). These results are in broad agreement with the literature on humidity's effect on building energy[14–21,42–44]. These hotspot regions with dominant latent heat load are also projected to experience strong urbanization[45,46] and rapid increase in AC adoption[47], making accurate energy projections crucial for energy infrastructure planning. Summer AC demand may be severely underestimated in these regions if energy projections are made using temperature-only metrics without accounting for the humidity effect.

Furthermore, we observe a spatially diverging pattern in changes of latent heat load fraction globally (Fig. 1f). Under this climate realization, 36% of the global urban area is projected to experience a decrease in latent heat load fraction, while 59% is projected to undergo an increase. Cities in coastal South America, Nova Scotia, southern and eastern Africa, western India and southwest China may experience an increase in latent heat load fraction of up to 85%, whereas cities in equatorial Africa, Southeast Asia, Central America and northeast China may

 https://doi.org/10.1038/s44284-026-00474-4

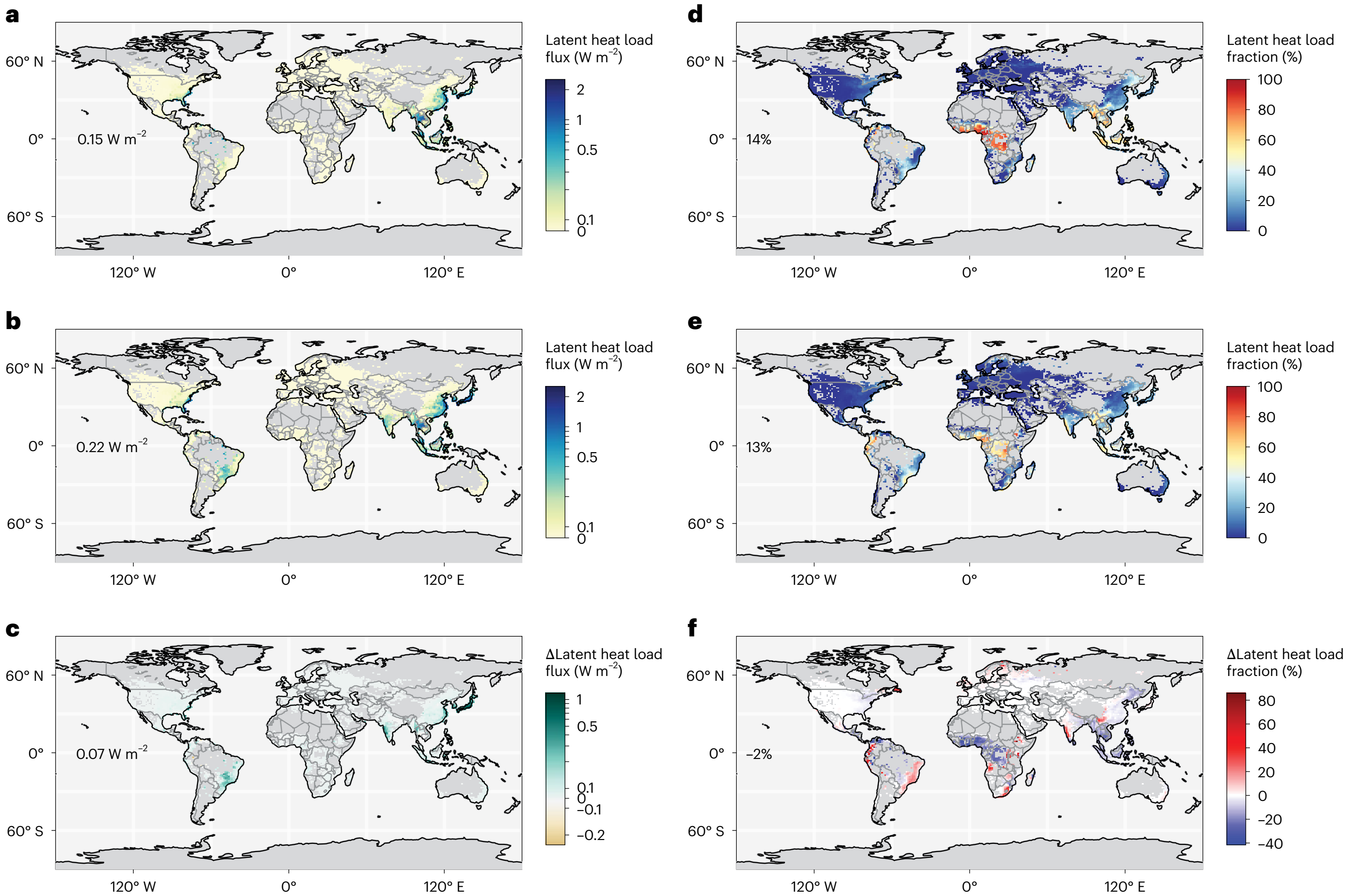

Fig. 1 | Latent heat load increases under climate change but becomes spatially divergent in its contribution to AC energy demand. **a**,**b**, Average summer latent heat load flux (with respect to urban area) for the first decade (2015–2024; **a**) and the last decade (2090–2099; **b**) of the simulation period. **c**, The difference in latent heat load flux between the last decade and the first decade. **d**,**e**, Average summer latent heat load fraction (latent heat load as a fraction of total AC energy demand, expressed in percentage) for the first decade (**d**) and the last decade (**e**). **f**, The difference in latent heat load fraction between the last decade and the first decade. The numbers annotated to the left of the domain in **a**–**c** represent the global area-weighted mean, and in **d**–**f** the global arithmetic mean. In the Northern Hemisphere, summer is assumed to be from June to August and winter from December to February; seasons are assumed to be flipped for the Southern Hemisphere. Basemap from Natural Earth (https://www.naturalearthdata.com/).

see up to 41% decrease. Changes in latent heat load fraction reflects the competing effect of urban warming and urban (de)humidification[48,49]: an increase in latent heat load fraction means the city is humidifying 'faster' than it is getting warmer, and a decrease means either the city is warming 'faster' than it is becoming more humid, or the city is becoming both warmer and drier. This diverging pattern of latent heat load fraction highlights the challenge of making future energy projections from present-day energy use and temperature relationships: as latent heat load fraction changes under climate change, so does the AC energy–temperature relationship. Extrapolating based on the current local AC energy–temperature relationship into the future may either overestimate (if latent heat load fraction decreases over time) or underestimate (if latent heat load fraction increases) humidity-driven AC energy demand depending on the competing effect of local urban warming and humidification. This further illustrates the critical importance of dynamically modeling the humidity effect in future energy projections.

Temperature–humidity interplay shapes urban building energy design space

As humidity's effect on AC energy demand diverges among global cities, each city will face a unique shift in the design conditions for indoor thermal comfort, which we will refer to as their building energy design space. We illustrate the shifts and the mechanisms behind them using six cities (see locations in Extended Data Fig. 2) that fall on the spectrum of changes in latent heat load fraction (Fig. 2a).

When latent heat load becomes more dominant in a city (Fig. 2b,c), it is an indication that the city is getting hotter and more humid under climate change, but different mechanisms could be at play. The city's relative humidity may be increasing as well as its temperature, such as in São Paulo, Brazil (Fig. 2c). Alternatively, even when a city's relative humidity distribution does not change much, such as in Hubli, India (Fig. 2b), its latent heat load fraction may still increase substantially. This is because under Hubli's present-day climate, most summer days are humid but cool, so no AC use is required. In the future, climate change will increase its summer temperatures to such an extent that most humid days will be just hot enough to require AC use. These mildly hot but highly humid summer days dominate Hubli's cooling season, requiring more energy for dehumidification than for cooling (latent heat load fractions >90%), leading to a substantial increase in the average latent heat load fraction. This is consistent with our observation that moderately warm but highly humid days can increase AC energy demand by three times or more (see discussion in Fig. 4). It may soon become necessary for Hubli to design new buildings and AC systems with dehumidification in mind to prepare for both climate change and rapid urban expansion[50].

https://doi.org/10.1038/s44284-026-00474-4

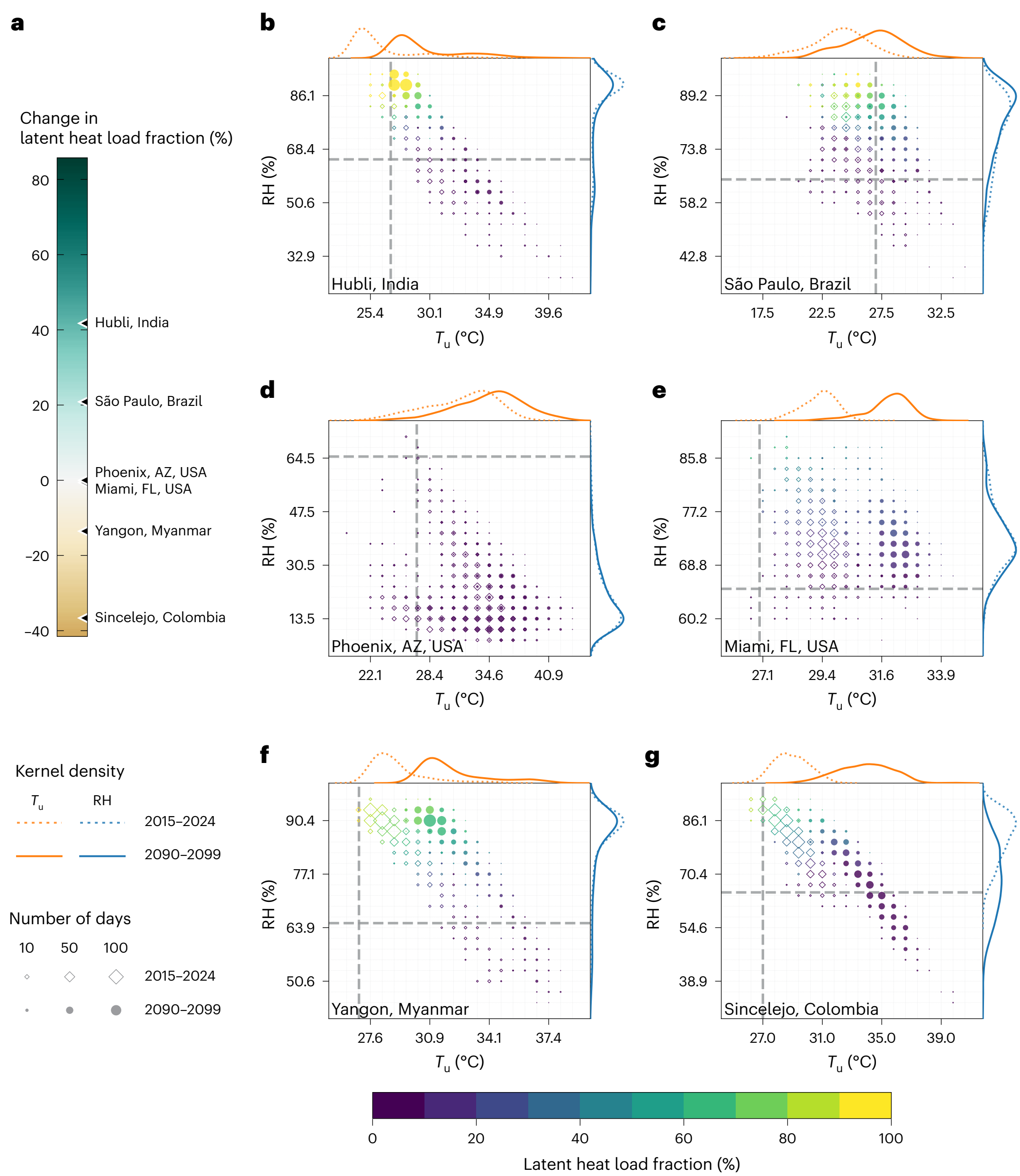

Fig. 2 | The interplay of temperature and humidity changes determines shifts in the building energy design space under future climates. a, The location of the six cities on the spectrum of changes in latent heat load fraction between the last decade (2090–2099) and the first decade (2015–2024), as presented in Fig. 1f. **b**–**g**, The distribution of average daily latent heat load fraction across urban 2-m temperature (T_u) and RH for the six cities, Hubli (**b**), São Paulo (**c**), Phoenix (**d**), Miami (**e**), Yangon (**f**), and Sincelejo (**g**), for 2015–2024 (unfilled diamonds) and 2090–2099 (filled circles). The size of the marker represents the number of days, and the color represents the average daily latent heat load fraction (bottom color bar) at the given T_u and RH bins. The kernel density distributions of T_u (orange lines, top of panels) and RH (blue lines, right of panels) are also presented for 2015–2024 (dotted lines) and 2090–2099 (solid lines). The indoor AC temperature setpoint (27 °C) and RH setpoint (65%) used in our model are denoted by dashed gray lines in each panel. They serve as proxies for evaluating the city's climate in relation to their needs for cooling and dehumidification.

Cities with virtually no change in their latent heat load fractions could be very dry (for example, Phoenix, USA; Fig. 2d) or very humid (for example, Miami, USA; Fig. 2e). Dry cities that stay dry do not need dehumidification now or in the future. For cities that are hot and humid in the present day, such as Miami, the majority of their cooling season has temperatures well above the threshold for requiring AC use, so the increase in temperature does not shift their latent heat load fraction much under climate change.

Cities where sensible heat load becomes more dominant (Fig. 2f,g) may experience essentially the reverse of the mechanisms as those whose latent heat load becomes more dominant. Their relative humidity may be decreasing (such as Sincelejo, Colombia; Fig. 2g). Alternatively, the city's relative humidity may remain unchanged, but its temperatures are increasing and moving further away from the threshold temperatures that trigger AC use (such as Yangon, Myanmar; Fig. 2f), thus making sensible heat load more dominant.

These results demonstrate that neither temperature nor humidity alone is sufficient for evaluating future shifts in building energy design space. Both metrics as well as their interactions with building energy use need to be taken into account to inform possible changes in future design. If run with alternative climate realizations (for example, different warming scenarios, or with perturbed initial conditions), our global physics-based dynamic model will allow us to identify cities where latent heat load will become increasingly important under

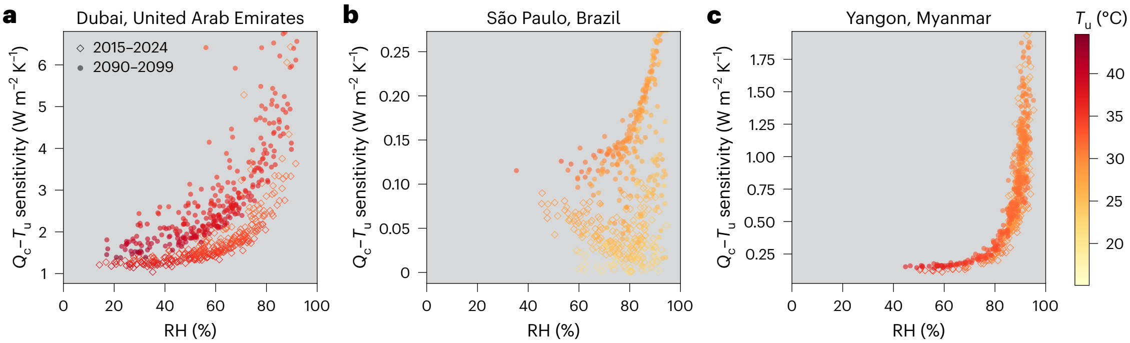

Fig. 3 | High humidity leads to exponential growth in AC energy–temperature (Q_C–T_u) sensitivity. a–c, Q_C–T_u sensitivity for Dubai (**a**), São Paulo (**b**) and Yangon (**c**), for summer days where $Q_C > 0.001$ W m^{-2} in 2015–2024 (unfilled diamonds) and in 2090–2099 (filled circles). The Q_C–T_u sensitivity is calculated for each day where the daily mean $Q_C > 0.001$ W m^{-2}. It is calculated as the daily mean Q_C divided by the difference between the daily mean T_u and the minimum of the daily mean T_u on days that satisfy $Q_C > 0.001$ W m^{-2} in each decade. The Q_C threshold is chosen for illustrative purposes only to prevent numerical instability caused by small temperature differences. For clarity, 33% of points that satisfy the above criteria are randomly selected from each decade for the plot.

uncertainties of climate change pathways and the internal variabilities of Earth systems. Targeted local studies can then be conducted to generate future weather files for building energy simulations, inform adoption of dehumidification technologies (for example, incorporating dehumidification control in cooling systems, providing portable desiccant units and so on), or guide modifications to building codes and design standards for future-proof buildings and energy systems[8].

Exponential increase in energy–temperature sensitivity with humidity

On warm days, the sensitivity of AC energy demand to urban temperature (Q_C–T_u sensitivity) increases exponentially with relative humidity due to latent heat load, regardless of climate zones. We illustrate this with three cities (see locations in Extended Data Fig. 2) below, spread across arid, temperate and tropical climate zones (Fig. 3a–c, respectively).

For cities with warm to hot summers, the Q_C–T_u sensitivity increases exponentially on humid days (roughly days with RH of 70% or above) once dehumidification becomes necessary (Fig. 3), regardless of climate zones. Under similar temperatures, the AC energy demand could be two to seven times more sensitive to urban temperature on a day with 80–90% humidity than on a day with <60% humidity. This means that urban energy demand extremes driven by high temperatures may be further exacerbated by high humidity, posing higher than anticipated risks to energy infrastructure if only sensible heat load is accounted for in demand forecasts. This is further compounded by the fact that climate change (or warmer temperatures) increases Q_C–T_u sensitivity through the positive biophysical feedbacks[6], where increase in AC energy use produces more waste heat, raising urban temperature and further increasing AC energy demand. This can be observed clearly for Dubai, where the Q_C–T_u sensitivity is 0.5 to 2 W m^{-2} K^{-1} higher in 2090–2099 than in 2015–2024 for every humidity level (Fig. 3a). This means that, for some cities, the impact of humidity on AC energy demand will be exacerbated by climate change, and latent heat load will become increasingly more important to account for in building design, energy planning and climate risk assessments. Such considerations need to extend beyond cities in more humid climate zones and include any cities that may experience hot and humid days.

We also observe a small number of cities where the relationship between Q_C–T_u sensitivity and RH is not apparent (Extended Data Fig. 3c) or negative (Extended Data Fig. 3a,b). However, this does not mean latent heat load is decreasing with increasing humidity. There are a few possible reasons for this: (1) the city has exclusive dry and hot summer days (Extended Data Fig. 3a) and, thus, no dehumidification is necessary; (2) the summer days are either hot and dry (do not need dehumidification) or cool and wet (do not need much cooling) (Extended Data Fig. 3b); and (3) the city has moderate temperature and humidity in summer (Extended Data Fig. 3c) and rarely needs cooling or dehumidification. It is worth noting that Dubai (Fig. 3a) and Phoenix (Extended Data Fig. 3a) are both classified as having an arid desert climate (Köppen–Geiger climate zone Bwh), and São Paulo (Fig. 3b) and Bologna (Extended Data Fig. 3b) both have a temperate climate with no dry season (Köppen–Geiger climate zone Cfa). This demonstrates that, although climate zone classifications can group cities by their mean climatology, the nuanced differences in their climate characteristics, their paths under climate change, and their unique urban characteristics could shape the cities' energy response very differently (see Supplementary Note 3 for a detailed discussion).

Unanticipated humidity-driven AC demand spikes

Humidity-driven AC demand increase will not only intensify energy demand extremes on hot days, but also cause substantial increase in demand on mildly hot but highly humid days. These demand spikes are probably missed if the projected demand was based solely on temperature. Here, we compare average daily Q_C on humid (daily mean RH >70%) versus non-humid (daily mean RH ≤70%) days with similar temperatures (falling within the same integer temperature bin). By comparing AC energy demand on days with similar temperatures, we can ensure a similar sensible heat load and therefore delineate the humidity effect.

In 2015–2024 on mildly hot days (27–28 °C) (Fig. 4a), humid days double Q_C (relative difference ≥100%) for cities in Eastern China, South America, parts of Midwest USA and southeast coast of Australia, and more than triple Q_C (relative difference ≥200%) for cities in equatorial Africa, North India and most of Southeast Asia, where latent heat load on average accounts for more than half of AC energy demand (Fig. 1d). The relative differences are reduced as temperature gets higher (Fig. 4b,c). This is the result of a combination of an increased Q_C on non-humid days due to high sensible heat load and a reduced Q_C on humid days due to reduced water content (as discussed later in this section). The area affected also shrinks under higher temperatures as fewer cities can reach both high temperature and high humidity simultaneously. By the end of the century, the humidity-driven demand increase becomes stronger in all three temperature bins (Fig. 4d–f). This is because, under climate change, the radiative heating of the surface and the atmosphere by greenhouse gas forcing increases the surface energy input, thereby increasing both temperature and humidity[24], as long as there is water available for evapotranspiration. This leads to an increase in the difference in excess water content (that is, amount of moisture that needs to be removed from the indoor air to satisfy the RH setpoint) between humid and non-humid days for each corresponding temperature bin

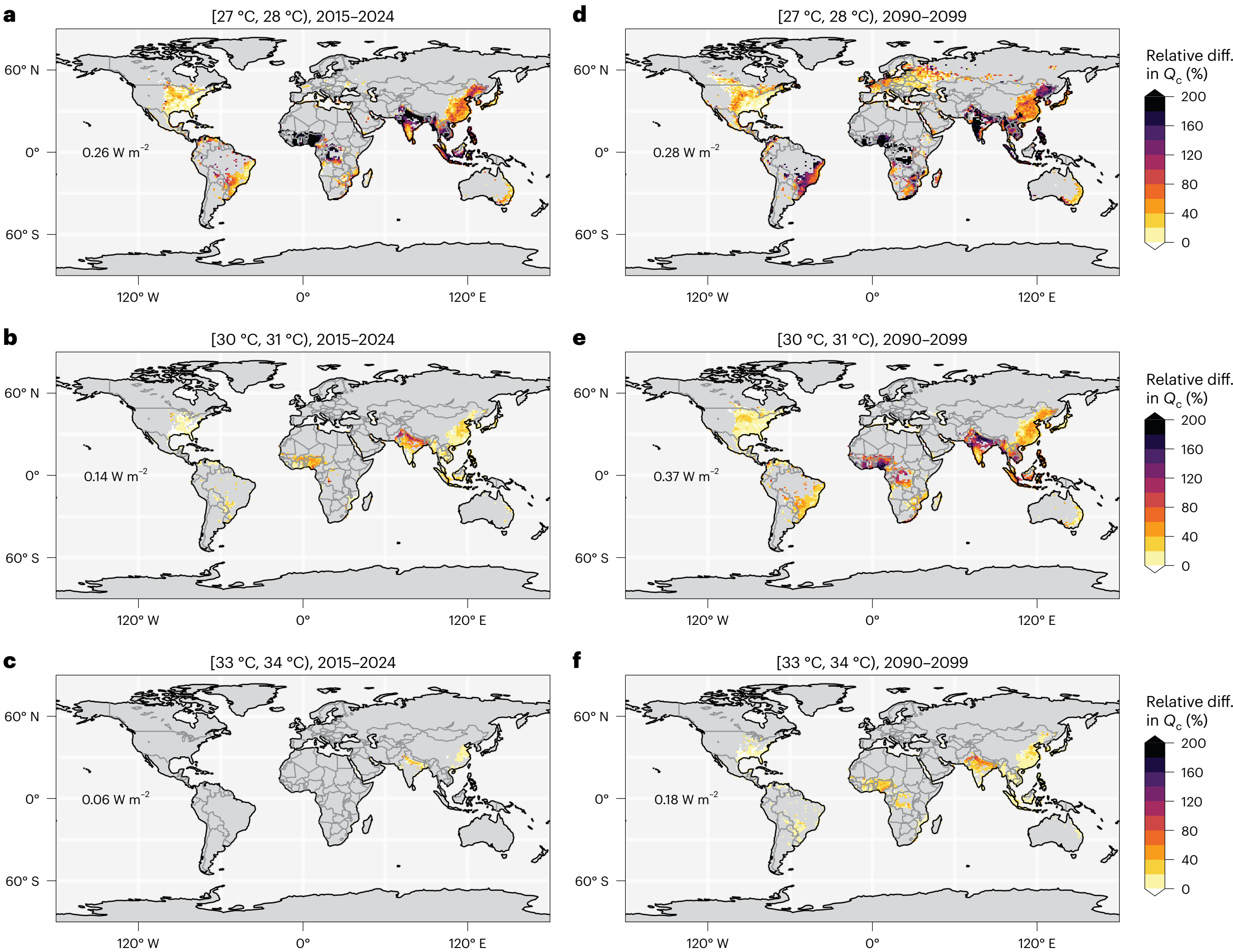

Fig. 4 | AC energy demand is two to three times higher on mildly hot but highly humid days. a–f, Difference (diff.) in average Q_C between humid days (RH >70%) and non-humid days (RH ≤70%) relative to the average Q_C on non-humid days, for temperatures between 27 °C and 28 °C (**a**,**d**), 30 °C and 31 °C (**b**,**e**) and 33 °C and 34 °C (**c**,**f**), in 2015–2024 (**a**–**c**) and 2090–2099 (**d**–**f**). The numbers in the subpanels represent the global area-weighted mean differences in average Q_C between humid days and non-humid days. Note that the temperature bins and humidity thresholds selected are informed by the temperature and humidity setpoints in our model simulation. They are used to illustrate the trends and enable comparisons between cases. The conclusions drawn will still be applicable to different sets of setpoints and thresholds. Basemap in **a**–**f** from Natural Earth (https://www.naturalearthdata.com/).

in the last decade compared with the first decade (Extended Data Fig. 4a versus Extended Data Fig. 4b) and, thus, an increased difference in AC energy required to remove this water. The increased surface energy input also enables more cities to achieve high humidity and high temperature simultaneously, leading to an expansion in the affected area within the same temperature bins.

Two competing factors influence the magnitude of global mean Q_C differences between humid and non-humid days (numbers annotated in each subpanel of Fig. 4). (1) Higher energy requirement. When outdoor relative humidity stays the same, more energy is required for dehumidification on hotter days. This is because both the excess water to be removed and the heat capacity of humid air increase with temperature. As a result, more energy is needed to condense the additional water and cool the higher-heat-capacity air at elevated temperatures. (2) Reduced excess water content. As temperature increases, fewer days can reach as high of a humidity (both absolute and relative) as in lower temperature days, which reduces the difference in excess water content between humid and non-humid days. This is because the partitioning of the surface energy budget into sensible and latent heat fluxes shifts toward sensible heat under higher-temperature days in urban areas. Water is usually limited in cities owing to the large fraction of impervious surfaces and cannot support sufficient evapotranspiration to raise humidity on hotter days[51]. As a result, the higher-temperature humid days tend to have smaller amounts of excess water in the air than lower-temperature humid days (Extended Data Fig. 4a,b; compare the three distributions within each subpanel) and therefore require less energy to remove this water. These factors counteract each other, leading to the observed trends in global mean Q_C differences with respect to temperature (see the annotated numbers in Fig. 4 and Extended Data Fig. 4c): In 2015–2024, global mean Q_C is higher by 0.26, 0.14 and 0.06 W m^{-2} on humid days than on non-humid days in 27–28 °C, 30–31 °C and 33–34 °C bins, respectively (Fig. 4a–c). The effect of reduced excess water content dominates over the higher energy requirement, forming a decreasing trend of global mean Q_C differences as temperature increases. In 2090–2099, the global mean Q_C differences increase from 0.28 W m^{-2} to 0.37 W m^{-2} going from 27 °C to 31 °C, then decrease to 0.18 W m^{-2} in the 33–34 °C bin. The higher surface energy availability under climate change may mobilize water vapor transport from the oceans through enhanced atmospheric circulation[52], delaying the reduction in excess water content to higher temperatures. This allows the effect of higher energy requirement to dominate between 27 °C and 31 °C, thus increasing global mean Q_C differences, before the reduction in excess water content takes hold and reduces global mean Q_C differences from 31 °C onward (Extended Data Fig. 4c).

These results show that moderately hot days may see the largest humidity-driven increase in urban AC energy demand, and this effect is further worsened by climate change. This finding is consistent with regional studies on the humidity effect on electricity demand[15]. This suggests that the AC energy demand extremes may not always coincide with temperature extremes[53]. This challenges current practices in energy and climate risks studies that draw energy implications from analyzing climate variables only[54,55], or studying energy demand extremes using energy or statistical models driven by climate extremes only[10,38,56]. Building energy simulations based on the Extreme Meteorological Years where only temperature extremes are identified[57] may therefore miss demand spikes due to high humidity and lead to more frequent undesirable indoor conditions than planned. This further confirms the necessity of explicitly and dynamically modeling energy–climate interactions[41,53] to capture the energy extremes that do not coincide with climate extremes

Discussion and conclusion

In this study, we find urban building dehumidification energy increases globally under climate change, but its contribution to total urban AC energy demand (quantified by latent heat load fraction) becomes spatially divergent, which can alter cities' building energy design conditions substantially. These diverging shifts occur as a result of the interplay between urban temperature and humidity changes under climate change. High humidity drives exponential growth in AC energy–temperature sensitivity on hot and humid days for cities across diverse climate zones. Under competing factors, cities may see unanticipated demand spikes on mildly hot but highly humid days, and this effect is further amplified by climate change. These results highlight the importance of capturing the evolving and spatially diverging humidity effect on building energy for climate-sensitive building design and urban energy planning.

This study represents continued efforts in overcoming the disconnect between climate and energy modeling communities[53] by improving the representation of coupled human–urban–Earth dynamics in global Earth system models (ESMs). The results of this study can guide efforts in generating future weather files for building energy simulations, and help identify demand extremes driven by both temperature and humidity for electric grid resilience. Building dehumidification extends the urban climate–energy feedbacks into the water cycle and may dynamically interact with urban vegetation[50] and green infrastructure. Such interactions could influence urban water vapor–temperature feedback, which may play a major role in determining urban weather extremes such as humid heat and extreme precipitation. The latent heat load and dehumidification modeling scheme developed in this study adds to the capability of CESM in comprehensive climate risk assessments for both human and natural systems on a global scale, and providing physics-based, globally coherent results to guide local investigations and knowledge transfer in climate-aware building design and energy planning.

A few potential pathways may be explored to further evaluate the climate-driven humidity effect on building energy in cities. This study isolates climate change effects by keeping nonclimatic factors at the present-day level. These factors could strongly influence future AC energy demand[8,9]: expected increase in AC adoption rate and population, especially in the global south, will further drive future AC energy demand by increasing both the sensible and latent heat load, while AC efficiency improvements from technology development may mitigate the increase in energy consumption due to AC. In addition to influencing the total AC energy demand/consumption, some nonclimatic factors may sway the sensible vs latent heat load dynamics: urbanization (increase in urban impervious areas) tends to increase urban temperature but lower humidity[3], thereby decreasing latent heat load fractions, whereas urban greening may compensate for or revert this effect; improvements in building insulation, human acclimatation and behavioral adaptation (reflected in higher AC temperature setpoints) will primarily reduce sensible heat load, thus increasing latent heat load fraction. The modeling scheme also assumes that dehumidification is done by vapor compression systems as it is the most common dehumidification technology in use for residential and commercial buildings today[6,58]. Alternative dehumidification technologies (such as solid or liquid desiccant systems) will have different energy requirements but will be similarly affected by the increasing demand for dehumidification under climate change. These dynamics can be modeled by supplying the associated socio-techno-economic projections to the current modeling scheme. Indoor moisture sources, such as cooking and showering, can be modeled or parameterized by integrating global data on occupants' behavior once available. These factors are less climate-sensitive but will help provide a more complete picture of humidity-driven building energy demand changes. In addition, future projections of the water cycle are often more uncertain than temperature projections[59,60]. It is thus worth exploring the results of this study under uncertainty from multiple climate realizations (modeled by multiple ESMs) and with multiple coupled simulations (multimember ensembles) for a more robust understanding of climate-driven humidity effects on building energy demand.

Methods

Overview of CLMU BEM and AC energy flux modeling

The model development in this study is based on the most recent version of Community Land Model Urban (CLMU)[61] (referred to hereinafter as CLMU5) with two important updates, namely the explicit AC adoption rate parameterization[41] and a new global continuous urban surface dataset[62]. We provide an overview on CLMU5, the new urban surface dataset and the integrated BEM and AC energy flux modeling below for the context of later sections.

The CLMU5 is a single-layer urban canopy model coupled with the Community Terrestrial System Model (CTSM), the land component of CESM. The CTSM uses a nested subgrid hierarchy in each grid cell to represent different land uses, and each grid cell can have up to seven land units including up to three urban land units as well as vegetated, crop, glacier and lake land units. The CLMU5 serves as the urban land parameterization for the urban land units. Within an urban land unit, a roof, walls (sunlit and shaded) and canyon floor surfaces (pervious and impervious) are organized in an urban canyon configuration.

The CLMU5 is constrained by a global surface properties dataset which includes morphological (for example, canyon height-to-street width ratio, roof fraction, average building height and pervious canyon floor fraction), radiative (for example, facet-level albedo and emissivity) and thermal (for example, heat capacity and thermal conductivity) urban surface properties. In this study, we choose to use U-Surf, the newly developed global 1 km spatially continuous urban surface property dataset for ESMs[62], aggregated to our desired resolution (0.9375° latitude × 1.25° longitude). U-Surf has been shown to reduce model biases and better capture the spatial heterogeneity of the urban surface than the default dataset (described in refs. 61,63) even after aggregation[62]. Moreover, the U-Surf dataset helps to reduce overestimation in simulated anthropogenic heat due to heating and AC from the default dataset (Supplementary Table 1) and is therefore chosen for this study.

The BEM in CLMU is a simplified dynamic model that can operate globally with sufficient accuracy and within the constraints of available global urban data. For each grid cell that has an urban area, an 'average building' is simulated to represent buildings in that area, with specified geometric, radiative and thermal properties based on the global urban surface dataset (U-Surf in this study). Processes that are accounted for in the BEM include heat conduction through building surfaces (roof, sunlit and shaded walls, and floor), convection (sensible heat exchange) between interior surfaces and indoor air, longwave radiation exchange between interior surfaces, and infiltration and exfiltration (at a fixed rate) (Extended Data Fig. 5a). The urban cooling and heating energy demand and urban climate variables are prognosed in each urban land unit based on the heat exchange processes between the 'average building' and its surroundings at a time step of 30 min.

Building AC energy demand can be directly output from the BEM. It is calculated as the amount of energy flux required to be removed to bring the interior building temperature down to the cooling setpoint temperature. The BEM assumes a single thermal zone and infinite-capacity heating and AC systems. The simulated results can thus be interpreted as 'cooling load/AC energy demand', that is, the amount of energy needed to keep the indoor conditions within the specified limits at the time step of the model. Note that the infinite-capacity assumption is not expected to substantially affect the simulation performance of the model at the timescale relevant to this study (see Supplementary Note 4 for more information). With the newly developed explicit AC adoption scheme[41], the AC energy demand is proportional to the AC adoption rate of a given location (Extended Data Fig. 5a). This development improves the anthropogenic heat modeling performance and better represents the socioeconomic dimension of urban energy demand. The model development in this study is based on the explicit AC adoption scheme. We note a potential overestimation in AC energy demand associated with this formulation in Supplementary Note 4 but do not believe it substantially impacts the model results for this work.

A new scheme for modeling latent heat load and dehumidification

High indoor humidity can promote the growth or survivability of harmful microorganisms[64,65] and may lead to indoor discomfort[66]. The recommended upper limit for indoor humidity is usually based on relative humidity and falls between 60% and 70% (refs. 64,67,68).

Dehumidification is a byproduct of AC cooling, regardless of the complexity of the AC equipment or system. During the cooling process, if the air is cooled to below its dew point temperature, water will condense on the evaporator coil, which effectively dehumidifies the air[6]. Some (more complex) AC systems are required to have dedicated humidity control (such as for offices, hospitals or schools), where humidity is maintained under the threshold with an additional desiccant system or by overcooling the supply air to desired humidity then reheating it[6].

In the original BEM in CLMU[61], indoor air is assumed to be completely dry. This means the energy flux due to infiltration/exfiltration (${F_{\mathrm{vent}}}^t$) considers only sensible heat exchanges:

$$ {F_{\mathrm{vent}}}^t = \left(\frac{\mathrm{ACH}}{3{,}600}\right) H {\rho_{\mathrm{dry}}}^t C_{p,\mathrm{dry}} \left({T_{\mathrm{canyon}}}^t - {T_{\mathrm{iB}}}^t\right), \tag{1} $$

where ACH represents the infiltration rate in the unit of air change per hour, with a default value of 0.3 (which means 0.3 times the volume of indoor air is replaced with outdoor air every hour) everywhere, H is building height (m), ${\rho_{\mathrm{dry}}}^t$ is dry air density (kg m^{-3}) calculated at local atmospheric pressure and indoor air temperature ${T_{\mathrm{iB}}}^t$ (K) at time step t, $C_{p,\mathrm{dry}} = 1.00464 \times 10^3$ is the specific heat of dry air (J kg^{-1} K^{-1}) and ${T_{\mathrm{canyon}}}^t$ is the urban canopy layer air temperature (K) at t.

The model then solves for ${T_{\mathrm{iB}}}^{t+1}$ and the four indoor surface (roof, sunlit wall, shaded wall and floor) temperatures through the energy balance equations for the indoor air and the four indoor surfaces. The heat transfer processes considered in the energy balances include infiltration/exfiltration calculated in equation (1), conduction through the roof and two walls (the floor is assumed to be adiabatic), convection between the indoor surfaces and indoor air, and longwave radiation between the indoor surfaces. Readers are referred to ref. 61 for more details.

Due to the dry-air assumption, dehumidification load calculation is not possible in the original BEM. The AC energy demand in the original BEM thus only considers the energy needed to cool (that is, reduce indoor temperature). When the indoor temperature at t+1 exceeds the temperature setpoint $T_{\mathrm{sat,max}}$ (that is, ${T_{\mathrm{iB}}}^{t+1} > T_{\mathrm{sat,max}}$; 'sat' denotes saturated/100% AC adoption[41]), the AC energy demand under saturated AC adoption, ${F_{\mathrm{sat,AC}}}^{t+1}$, is calculated as the excessive sensible heat to be removed by the infinite-capacity air conditioner in one time step:

$$ {F_{\mathrm{sat,AC}}}^{t+1} = \begin{cases} \frac{H {\rho_{\mathrm{dry}}}^t C_{p,\mathrm{dry}}}{\Delta t}\left({T_{\mathrm{iB}}}^{t+1} - T_{\mathrm{sat,max}}\right), & {T_{\mathrm{iB}}}^{t+1} > T_{\mathrm{sat,max}}; \\ 0, & \text{otherwise.} \end{cases} \tag{2} $$

The actual AC flux being removed from the indoor air, ${F_{\mathrm{AC}}}^{t+1}$, is scaled based on the AC adoption rate, p_{AC} (more details in ref. 31):

$$ {F_{\mathrm{AC}}}^{t+1} = p_{\mathrm{AC}} {F_{\mathrm{sat,AC}}}^{t+1}. \tag{3} $$

The indoor air temperature is then reset as follows:

$$ {T_{\mathrm{iB}}}^{t+1} = \frac{(1-p_{\mathrm{AC}}){F_{\mathrm{sat,AC}}}^{t+1}\Delta t}{H \rho_{\mathrm{dry}} C_{p,\mathrm{dry}}} + T_{\mathrm{sat,max}}, \text{ if } {F_{\mathrm{sat,AC}}}^{t+1} > 0. \tag{4} $$

In this study, operating under the constraints of a global climate model and the limited availability of global building systems and operations data (especially a lack of global data on dehumidification systems), we parameterize dehumidification energy demand (latent heat load) similarly to cooling energy demand (sensible heat load) using a setpoint approach (Extended Data Fig. 5b). This approach is also adopted by the BEMs in regional climate models[69]. We set an RH setpoint of 65% globally, following the recommendation of ASHRAE standards[67,68]. No humidification is considered. When AC use is triggered by temperature (that is, indoor dry-bulb air temperature exceeds the temperature setpoint; more details below), the model computes the energy required to remove the excess moisture (if any) by condensation as the latent heat load. As not all AC systems have dedicated humidity control, especially for residential applications, indoor humidity can often exceed 65% even with AC in operation[70]. The AC energy flux outputs in our modeling scheme thus should be considered as the energy required to maintain a healthy and comfortable indoor environment, and should not be thought of as the actual energy consumption for cooling or dehumidification, as the final energy consumption will depend on the type, design, availability of humidity control, and actual operations of the AC systems.

Latent heat load within the buildings comes from both outdoor and indoor sources: (a) outdoor latent heat being transported inside through ventilation or natural infiltration/exfiltration, and (b) indoor latent heat generated by human respiration and indoor activities (for example, cooking and showering)[69,71]. The parameterization in this study considers only the outdoor sources, as it is directly affected by the urban climate and the most sensitive to climate change.

Under the new modeling scheme, the energy flux due to infiltration/exfiltration into the building (${F_{\mathrm{vent}}}^t$) now consists of latent and sensible heat fluxes:

$$ \begin{aligned} {F_{\mathrm{vent}}}^t &= {F_{\mathrm{vent,sen}}}^t + {F_{\mathrm{vent,lat}}}^t \\ &= \left(\frac{\mathrm{ACH}}{3{,}600}\right) H {\rho_{\mathrm{humid}}}^t {C_{p,\mathrm{humid}}}^t \left({T_{\mathrm{canyon}}}^t - {T_{\mathrm{iB}}}^t\right) \\ &+ \left(\frac{\mathrm{ACH}}{3{,}600}\right) H {\rho_{\mathrm{humid}}}^t l_v \left({q_{\mathrm{canyon}}}^t - {q_{\mathrm{iB}}}^t\right), \end{aligned} \tag{5} $$

where ${\rho_{\mathrm{humid}}}^t$ is the humid air density (kg m^{-3}) calculated at local atmospheric pressure, indoor air temperature ${T_{\mathrm{iB}}}^t$ (K), and indoor specific

https://doi.org/10.1038/s44284-026-00474-4

humidity $q_{iB}{}^t$ (kg kg^{-1}) at t, $C_{p,\mathrm{humid}}{}^t$ is the specific heat of humid air (J kg^{-1} K^{-1}) (calculated from $C_{p,\mathrm{dry}}$, the specific heat of water vapor at 1.810×10^3 J kg^{-1} K^{-1}, and $q_{iB}{}^t$) at t, $l_v = 2.501 \times 10^6$ is the latent heat of vaporization of water (J kg^{-1}), and $q_{\mathrm{canyon}}{}^t$ is the urban canopy layer specific humidity (kg kg^{-1}) at t.

The sensible heat flux from infiltration affects indoor air temperature through the energy balance of indoor air and four interior surfaces as described above and in ref. 61. The moisture from infiltration affects the indoor specific humidity through mixing (assuming well mixed indoor air at each time step):

$$q_{iB}{}^{t+1} = q_{\mathrm{canyon}}{}^t\left(\frac{\mathrm{ACH}}{3{,}600}\Delta t\right) + q_{iB}{}^t\left(1 - \frac{\mathrm{ACH}}{3{,}600}\Delta t\right), \tag{6}$$

where t and t+1 denote two subsequent time steps, and Δt is the length of a time step (s).

We use indoor air temperature as the sole determinant for triggering AC energy use. This means AC energy flux will only be calculated if indoor air temperature goes over the temperature setpoint, but will not be calculated if only indoor humidity is over the humidity setpoint. This assumption is reasonable because the majority of AC controls are by temperature only, and the humidity dependence of AC energy use is evident only after urban temperature is high enough to trigger AC energy use[72].

When the indoor temperature exceeds the temperature setpoint $T_{\mathrm{sat,max}}$ (that is, $T_{iB}{}^{t+1} > T_{\mathrm{sat,max}}$), the sensible heat load, $F_{\mathrm{sat,AC,sen}}{}^{t+1}$, is calculated in the same way as in the original scheme in equation (2):

$$F_{\mathrm{sat,AC,sen}}{}^{t+1} = \begin{cases} \frac{H\rho_{\mathrm{humid}}{}^t C_{p,\mathrm{humid}}{}^t}{\Delta t}\left(T_{iB}{}^{t+1} - T_{\mathrm{sat,max}}\right), & T_{iB}{}^{t+1} > T_{\mathrm{sat,max}}; \\ 0, & \text{otherwise.} \end{cases} \tag{7}$$

To evaluate whether dehumidification is needed, we first convert the RH setpoint to a specific humidity setpoint, $q_{\mathrm{sat,max}}{}^{t+1}$, based on indoor air temperature and air pressure at t+1, using a built-in function that approximates saturation vapor pressure using a polynomial fit[73]. After that, the model evaluates indoor humidity, $q_{iB}{}^{t+1}$, against $q_{\mathrm{sat,max}}{}^{t+1}$. If $q_{iB}{}^{t+1} > q_{\mathrm{sat,max}}{}^{t+1}$, then the latent heat load is calculated as the excessive latent heat to be removed:

$$F_{\mathrm{sat,AC,lat}}{}^{t+1} = \begin{cases} \frac{H\rho_{\mathrm{humid}}{}^t l_v}{\Delta t}\left(q_{iB}{}^{t+1} - q_{\mathrm{sat,max}}\right), & T_{iB}{}^{t+1} > T_{\mathrm{sat,max}} \text{ and } q_{iB}{}^{t+1} > q_{\mathrm{sat,max}}; \\ 0, & \text{otherwise.} \end{cases} \tag{8}$$

The total AC energy demand under saturated (100%) AC adoption, $F_{\mathrm{sat,AC}}{}^{t+1}$, is then the sum of the latent and sensible heat load components calculated in equations (7) and (8):

$$F_{\mathrm{sat,AC}}{}^{t+1} = F_{\mathrm{sat,AC,sen}}{}^{t+1} + F_{\mathrm{sat,AC,lat}}{}^{t+1} = \begin{cases} \frac{H\rho_{\mathrm{humid}}{}^t C_{p,\mathrm{humid}}{}^t}{\Delta t}\left(T_{iB}{}^{t+1} - T_{\mathrm{sat,max}}\right), & T_{iB}{}^{t+1} > T_{\mathrm{sat,max}} \text{ and } q_{iB}{}^{t+1} \le q_{\mathrm{sat,max}}; \\ \frac{H\rho_{\mathrm{humid}}{}^t C_{p,\mathrm{humid}}{}^t}{\Delta t}\left(T_{iB}{}^{t+1} - T_{\mathrm{sat,max}}\right) + \frac{H\rho_{\mathrm{humid}}{}^t l_v}{\Delta t}\left(q_{iB}{}^{t+1} - q_{\mathrm{sat,max}}\right), & T_{iB}{}^{t+1} > T_{\mathrm{sat,max}} \text{ and } q_{iB}{}^{t+1} > q_{\mathrm{sat,max}}; \\ 0, & \text{otherwise.} \end{cases} \tag{9}$$

It is assumed that the latent and sensible heat fluxes removed by AC are converted to sensible heat before being released into the urban canyon. This assumption is adopted by most regional scale studies using the Weather Research and Forecasting model[69] and true for most AC systems in use today[33]. Heat removed by air conditioners may be partially rejected as latent heat (for example, through the use of cooling towers) in large commercial applications, which is not currently considered in the model.

The actual AC flux being removed from the indoor air, $F_{\mathrm{AC}}{}^{t+1}$, is scaled based on the AC adoption rate in the same way as equation (3).

The model also computes actual sensible heat load flux ($F_{\mathrm{AC,sen}}{}^{t+1}$) that can be output from the model for further analysis. The actual latent heat load flux ($F_{\mathrm{AC,lat}}{}^{t+1}$) is then the difference between total actual AC flux and sensible heat load flux:

$$F_{\mathrm{AC,sen}}{}^{t+1} = p_{\mathrm{AC}} F_{\mathrm{sat,AC,sen}}{}^{t+1}, \tag{10}$$

$$F_{\mathrm{AC,lat}}{}^{t+1} = F_{\mathrm{AC}}{}^{t+1} - F_{\mathrm{AC,sen}}{}^{t+1}. \tag{11}$$

The indoor air temperature and specific humidity are then reset as follows:

$$T_{iB}{}^{t+1} = \frac{(1-p_{\mathrm{AC}})F_{\mathrm{sat,AC,sen}}{}^{t+1}\Delta t}{H\rho_{\mathrm{humid}}{}^t C_{p,\mathrm{humid}}{}^t} + T_{\mathrm{sat,max}}, \text{ if } F_{\mathrm{sat,AC,sen}}{}^{t+1} > 0; \tag{12}$$

$$q_{iB}{}^{t+1} = \frac{(1-p_{\mathrm{AC}})F_{\mathrm{sat,AC,lat}}{}^{t+1}\Delta t}{H\rho_{\mathrm{humid}}{}^t l_v} + q_{\mathrm{sat,max}}, \text{ if } F_{\mathrm{sat,AC,lat}}{}^{t+1} > 0. \tag{13}$$

The removed water (condensate) flux, $q_{\mathrm{condensate}}{}^{t+1}$, with a unit of kg m^{-2} s^{-1} or mm s^{-1}, is computed at the end of each time step as

$$q_{\mathrm{condensate}}{}^{t+1} = \max\left[0, \left(q_{iB}{}^t - q_{iB}{}^{t+1}\right)\right]\frac{H\rho_{\mathrm{humid}}{}^t}{\Delta t}. \tag{14}$$

To ensure total water remains conserved in the model, we assume that the condensate is drained through the sewer systems. As sewer systems are not explicitly modeled in CTSM, we approximate this behavior by sending the condensate to urban surface runoff, which is then sent to the river model of CTSM. The additional runoff contributes to less than 0.004% of increase in flow rate for the 50 largest rivers (by volume) in the world (Supplementary Table 2).

Validation

We validate the new scheme on its performance in simulating total AC energy demand and latent heat load. To do this, we conduct two global land-only simulations (that is, the CTSM is active, while other components of CESM such as atmosphere, ocean and sea ice use prescribed data) under present-day climate conditions at 0.9375° latitude × 1.25° longitude spatial resolution. The simulations are run from 2000 to 2014 driven by atmospheric forcing (precipitation, incoming solar and longwave radiation, and air temperature, humidity, wind and CO_2 concentration at the lowest atmospheric model layer) from the Global Soil Wetness Project forcing dataset (GSWP3) (3-hourly, 0.5°; http://hydro.iis.u-tokyo.ac.jp/GSWP3/)[74]. One simulation uses the updated CLMU scheme developed in this study ('with dehum.'), while the other uses the original CLMU scheme ('no dehum.'). We output total AC energy demand from both simulations, and the sensible heat load and latent heat load components of total AC energy demand from the 'with dehum.' simulation at monthly intervals, then compare the simulated results with observation-based datasets as well as modeling case studies from the literature, as detailed below.

Anthropogenic heat flux due to AC. To validate total AC energy demand in a spatially explicit manner, we compare the simulated anthropogenic heat flux (AHF) due to AC with that derived from gridded observational datasets. Because all energy consumption eventually ends up as anthropogenic heat into the climate system, we can indirectly validate simulated AC energy demand by converting it to AC energy consumption, then comparing the AC energy consumption with observationally estimated AHF. The procedure follows that in ref. 41, except in this study we leverage an updated AHF dataset from the authors of ref. 75 and correspondingly update our estimates for AC energy fractions. Details are provided in Supplementary Note 5. For the 15 countries/regions where validation data are available, our parameterization ('With dehum.') simulates AHF due to AC reasonably well, and slightly improves the total AHF and spatial correlation as compared with the original scheme with no dehumidification ('No dehum.') (Extended Data Figs. 6 and 7). This demonstrates that our new scheme can simulate well the magnitude and spatial distribution of the total AC energy demand on a large scale.

At the grid-cell level, most grids see virtually no change in AHF due to AC between 'With dehum.' and 'No dehum.' (Extended Data Figs. 6 and 7 and Supplementary Table 3). This is to be expected, as most of the grids for which validation data are available have low dehumidification needs (latent heat load fractions <20%; Fig. 1d). Some cities show an improvement (for example, New York, USA; Chicago, USA; Nagoya, Japan), while some cities depart further from the observational estimates (for example, Houston, USA; Tokyo, Japan; Osaka, Japan). This does not necessarily indicate an error in the modeling scheme, but rather a larger deviation from our assumption of 'maintaining indoor comfort and health': in reality, not all AC systems have dedicated humidity control, especially in residential applications, leading to indoor humidity frequently exceeding 65%, the RH setpoint assumed in this study[70]. In other words, the AC energy consumption derived from the simulated AC energy demand reflects the energy consumption required to maintain a healthy and comfortable indoor environment, which may not currently be achieved by the AC systems in place and thus not reflected in the observational estimates.

Latent heat load fraction. We compare our simulated latent heat load fractions from the 'With dehum.' simulation with a few case studies found in the literature, which represent the relative magnitude of latent heat load as a fraction of total AC energy demand (Extended Data Table 2). Note that this validates 'latent heat load', the amount of latent heat needed to be removed to satisfy the design condition (that is, an RH setpoint), which is the same definition as the latent heat load computed by our model. This means that the validation performance for latent heat load should not be affected by our setpoint approach. Results show that our parameterization is reasonable in reproducing the dehumidification energy demand relative to total AC energy demand as modeled by more detailed BEMs. This shows that our new scheme, although built in a simplified urban BEM, can well capture the first-order dynamics of latent and sensible heat loads at local scales.

Simulation
We conduct a global land-only simulation at 0.9375° latitude × 1.25° longitude spatial resolution to project future urban climate and energy demand under a climate change scenario. We chose one of the most plausible Shared Socioeconomic Pathway-Representative Concentration Pathway (SSP-RCP) scenarios, SSP3-7.0, which represents regional rivalry and high greenhouse gas emissions. This helps illustrate the 'worst case scenario' in climate change and its related impacts. The simulation period is from 2015 to 2099 driven by atmospheric forcings from a fully coupled CESM2 simulation. The fully coupled simulation captures the large-scale dynamics between atmosphere, ocean, land and so on. Using atmospheric conditions from the fully coupled simulation to drive the land-only simulation allows us to replicate enhanced atmospheric circulation and water vapor transport driven by climate change[52] and simulate the effect of dehumidification under such changes. We keep the nonclimatic conditions (AC adoption rate, technology, urban extent and building stock) constant throughout the simulation period, which allows us to delineate the climate-only effect on humidity and dehumidification energy.

Latent heat load fraction
Latent heat load fraction quantifies the relative contribution of dehumidification energy as a fraction of total AC energy demand (expressed in percentage form). In this study, we calculate the latent heat load fraction using daily averaged output of dehumidification and AC energy demand. For a given grid cell i on a given day d, it is calculated as

$$\text{latent heat load fraction}_i^d = \frac{F_{\mathrm{AC,lat}_i}^{\;d}}{F_{\mathrm{AC}_i}^{\;d}} \times 100\%. \tag{15}$$

$F_{\mathrm{AC,lat}_i}^{\;d}$ is the simple average of $F_{\mathrm{AC,lat}_i}^{\;t}$ for all timesteps in a day, and $F_{\mathrm{AC}_i}^{\;d}$ the simple average of all $F_{\mathrm{AC}_i}^{\;t}$. From equations (3), (10) and (11), we know that both $F_{\mathrm{AC,lat}_i}^{\;t}$ and $F_{\mathrm{AC}_i}^{\;t}$ are scaled by the same AC adoption rate, p_{AC_i} and, thus, p_{AC_i} is canceled out in the division. Latent heat load fraction is therefore independent of AC adoption rate. This means that, while our simulation assumes a constant AC adoption rate for each grid cell throughout the simulation period, our analysis and conclusions on latent heat load fractions should still hold under changing AC adoption rates.

Reporting summary
Further information on research design is available in the Nature Portfolio Reporting Summary linked to this article.

Data availability
The CESM simulation results that support the findings of this study are available via Zenodo at https://doi.org/10.5281/zenodo.20563953 (ref. 76). Source data are provided with this paper.

Code availability
The code base used to perform the CESM simulations is available via GitHub at https://github.com/cathyxinchangli/CTSM/tree/dehumidification.

References

1. Raymond, C., Matthews, T. & Horton, R. M. The emergence of heat and humidity too severe for human tolerance. *Sci. Adv.* **6**, eaaw1838 (2020).
2. Yang, J., Zhao, L. & Oleson, K. Large humidity effects on urban heat exposure and cooling challenges under climate change. *Environ. Res. Lett.* **18**, 044024 (2023).
3. Zhang, K. et al. Increased heat risk in wet climate induced by urban humid heat. *Nature* **617**, 738–742 (2023).
4. Wang, P., Yang, Y., Tang, J., Leung, L. R. & Liao, H. Intensified humid heat events under global warming. *Geophys. Res. Lett.* **48**, e2020GL091462 (2021).
5. Speizer, S., Raymond, C., Ivanovich, C. & Horton, R. M. Concentrated and intensifying humid heat extremes in the IPCC AR6 regions. *Geophys. Res. Lett.* **49**, e2021GL097261 (2022).
6. Mujahid Rafique, M., Gandhidasan, P., Rehman, S. & Al-Hadhrami, L. M. A review on desiccant based evaporative cooling systems. *Renew. Sustain. Energy Rev.* **45**, 145–159 (2015).
7. Li, X., Zhao, L., Qin, Y., Oleson, K. & Zhang, Y. Elevated urban energy risks due to climate-driven biophysical feedbacks. *Nat. Clim. Change* **14**, 1056–1063 (2024).
8. Mastrucci, A., van Ruijven, B., Byers, E., Poblete-Cazenave, M. & Pachauri, S. Global scenarios of residential heating and cooling energy demand and CO_2 emissions. *Climatic Change* **168**, 14 (2021).

9. Wang, C. et al. Impacts of climate change, population growth, and power sector decarbonization on urban building energy use. *Nat. Commun.* **14**, 6434 (2023).
10. Sherman, P., Lin, H. & McElroy, M. Projected global demand for air conditioning associated with extreme heat and implications for electricity grids in poorer countries. *Energy Build.* **268**, 112198 (2022).
11. IPCC *Climate Change 2022: Impacts, Adaptation and Vulnerability* (eds Pörtner, H.-O. et al.) (Cambridge Univ. Press, 2023); https://doi.org/10.1017/9781009325844
12. Waite, M. et al. Global trends in urban electricity demands for cooling and heating. *Energy* **127**, 786–802 (2017).
13. Huang, J., Ritschard, R. L., Bull, J. C. & Chang, L. Climatic indicators for estimating residential heating and cooling loads. *ASHRAE Trans.* **93**, 72–111 (1987).
14. Maia-Silva, D., Kumar, R. & Nateghi, R. The critical role of humidity in modeling summer electricity demand across the United States. *Nat. Commun.* **11**, 1686 (2020).
15. Rastogi, D. et al. The role of humidity in determining future electricity demand in the southeastern United States. *Environ. Res. Lett.* **16**, 114017 (2021).
16. Cao, J., Li, M., Wang, M. & Li, B. Impacts of temperature and humidity changes on air-conditioning design load under the climate change conditions in different climate zones of China. *Meteorol. Appl.* **28**, e2026 (2021).
17. Cao, J., Li, M., Yang, X., Zhang, R. & Wang, M. The impact of urban dry island on building energy consumption is overlooked compared to urban heat island in cold climate. *Energy Build.* **320**, 114655 (2024).
18. Shi, L. et al. Impacts of urban microclimate on summertime sensible and latent energy demand for cooling in residential buildings of Hong Kong. *Energy* **189**, 116208 (2019).
19. Paolini, R. et al. The hygrothermal performance of residential buildings at urban and rural sites: sensible and latent energy loads and indoor environmental conditions. *Energy Build.* **152**, 792–803 (2017).
20. Zhai, Z. J. & Helman, J. M. Climate change: projections and implications to building energy use. *Build. Simul.* **12**, 585–596 (2019).
21. Kheiri, F., Haberl, J. S. & Baltazar, J.-C. Impact of outdoor humidity conditions on building energy performance and environmental footprint in the degree days-based climate classification. *Energy* **283**, 128447 (2023).
22. Wang, X. et al. Integration of moisture effects into urban building energy modeling. *Build. Simul.* **18**, 663–678 (2025).
23. IPCC *Climate Change 2021: The Physical Science Basis* (eds Masson-Delmotte, V. et al.) (Cambridge Univ. Press, 2023); https://doi.org/10.1017/9781009157896
24. Song, F., Zhang, G. J., Ramanathan, V. & Leung, L. R. Trends in surface equivalent potential temperature: a more comprehensive metric for global warming and weather extremes. *Proc. Natl Acad. Sci.USA* **119**, e2117832119 (2022).
25. Stoy, P. C., Roh, J. & Bromley, G. T. It's the heat and the humidity: the complementary roles of temperature and specific humidity to recent changes in the energy content of the near-surface atmosphere. *Geophys. Res. Lett.* **49**, e2021GL096628 (2022).
26. Auffhammer, M., Baylis, P. & Hausman, C. H. Climate change is projected to have severe impacts on the frequency and intensity of peak electricity demand across the United States. *Proc. Natl Acad. Sci. USA* **114**, 1886–1891 (2017).
27. Romitti, Y. & Sue Wing, I. Heterogeneous climate change impacts on electricity demand in world cities circa mid-century. *Sci. Rep.* **12**, 4280 (2022).
28. van Ruijven, B. J., De Cian, E. & Sue Wing, I. Amplification of future energy demand growth due to climate change. *Nat. Commun.* **10**, 2762 (2019).
29. Wenz, L., Levermann, A. & Auffhammer, M. North–south polarization of European electricity consumption under future warming. *Proc. Natl Acad. Sci. USA* **114**, E7910–E7918 (2017).
30. Isaac, M. & van Vuuren, D. P. Modeling global residential sector energy demand for heating and air conditioning in the context of climate change. *Energy Policy* **37**, 507–521 (2009).
31. Levesque, A. et al. How much energy will buildings consume in 2100? A global perspective within a scenario framework. *Energy* **148**, 514–527 (2018).
32. Mideksa, T. K. & Kallbekken, S. The impact of climate change on the electricity market: a review. *Energy Policy* **38**, 3579–3585 (2010).
33. Salamanca, F., Georgescu, M., Mahalov, A., Moustaoui, M. & Wang, M. Anthropogenic heating of the urban environment due to air conditioning. *J. Geophys. Res. Atmos.* **119**, 5949–5965 (2014).
34. Takane, Y., Kikegawa, Y., Hara, M. & Grimmond, C. S. B. Urban warming and future air-conditioning use in an Asian megacity: importance of positive feedback. *npj Clim. Atmos. Sci.* **2**, 39 (2019).
35. Kikegawa, Y., Nakajima, K., Takane, Y., Ohashi, Y. & Ihara, T. A quantification of classic but unquantified positive feedback effects in the urban-building-energy-climate system. *Appl. Energy* **307**, 118227 (2022).
36. Vahmani, P., Luo, X., Jones, A. & Hong, T. Anthropogenic heating of the urban environment: an investigation of feedback dynamics between urban micro-climate and decomposed anthropogenic heating from buildings. *Build. Environ.* **213**, 108841 (2022).
37. Hsieh, C.-M., Aramaki, T. & Hanaki, K. The feedback of heat rejection to air conditioning load during the nighttime in subtropical climate. *Energy Build.* **39**, 1175–1182 (2007).
38. Moazami, A., Nik, V. M., Carlucci, S. & Geving, S. Impacts of future weather data typology on building energy performance—investigating long-term patterns of climate change and extreme weather conditions. *Appl. Energy* **238**, 696–720 (2019).
39. *ANSI/ASHRAE Standard 169-2021: Climatic Data for Building Design Standards* (ASHRAE, 2021).
40. Mutasim Baba, F., Ge, H., Wang, L. (L.). & Zmeureanu, R. Assessing and mitigating overheating risk in existing Canadian school buildings under extreme current and future climates. *Energy Build.* **279**, 112710 (2023).
41. Li, X. et al. Enhancing urban climate–energy modeling in the Community Earth System Model (CESM) through explicit representation of urban air-conditioning adoption. *J. Adv. Model. Earth Syst.* **16**, e2023MS004107 (2024).
42. Fang, X., Winkler, J. & Christensen, D. Using EnergyPlus to perform dehumidification analysis on Building America homes. *HVAC&R Res.* **17**, 268–283 (2011).
43. Yoshino, H. et al. Indoor thermal environment and energy saving for urban residential buildings in China. *Energy Build.* **38**, 1308–1319 (2006).
44. Jin, Z. et al. Dehumidification load ratio: influence mechanism on air conditioning and energy saving potential analysis for building cooling. *Sustain. Cities Soc.* **99**, 104942 (2023).
45. Chakraborty, T. C. et al. Large disagreements in estimates of urban land across scales and their implications. *Nat. Commun.* **15**, 9165 (2024).
46. Gao, J. & O'Neill, B. C. Mapping global urban land for the 21st century with data-driven simulations and Shared Socioeconomic Pathways. *Nat. Commun.* **11**, 2302 (2020).
47. Auffhammer, M. & Mansur, E. T. Measuring climatic impacts on energy consumption: a review of the empirical literature. *Energy Econ.* **46**, 522–530 (2014).
48. Langendijk, G. S., Rechid, D. & Jacob, D. Urban areas and urban–rural contrasts under climate change: what does the EURO-CORDEX ensemble tell us?—Investigating near surface humidity in Berlin and its surroundings. *Atmosphere* **10**, 730 (2019).

49. Huang, X. & Song, J. Urban moisture and dry islands: spatiotemporal variation patterns and mechanisms of urban air humidity changes across the globe. *Environ. Res. Lett.* **18**, 103003 (2023).
50. Meili, N. et al. Modeling the effect of trees on energy demand for indoor cooling and dehumidification across cities and climates. *J. Adv. Model. Earth Syst.* **17**, e2024MS004590 (2025).
51. Zhao, L. et al. Interactions between urban heat islands and heat waves. *Environ. Res. Lett.* **13**, 034003 (2018).
52. Simpson, I. R. et al. Observed humidity trends in dry regions contradict climate models. *Proc. Natl Acad. Sci. USA* **121**, e2302480120 (2024).
53. Craig, M. T. et al. Overcoming the disconnect between energy system and climate modeling. *Joule* https://doi.org/10.1016/j.joule.2022.05.010 (2022).
54. Deroubaix, A. et al. Large uncertainties in trends of energy demand for heating and cooling under climate change. *Nat. Commun.* **12**, 5197 (2021).
55. Stanton, W. H., David, J. E. III, Jose, L. H., Christine, T. B. & Thomas, J. B. Responses of energy use to climate change: a climate modeling study. *Geophys. Res. Lett.* **33**, L17703 (2006).
56. Perera, A. T. D., Nik, V. M., Chen, D., Scartezzini, J.-L. & Hong, T. Quantifying the impacts of climate change and extreme climate events on energy systems. *Nat. Energy* **5**, 150–159 (2020).
57. Machard, A. et al. Typical and extreme weather datasets for studying the resilience of buildings to climate change and heatwaves. *Sci. Data* **11**, 531 (2024).
58. Venegas, T. et al. Review of liquid desiccant air dehumidification systems coupled with heat pump: system configurations, component design, and performance. *Energy Build.* **279**, 112655 (2023).
59. Douville, H. & Willett, K. M. A drier than expected future, supported by near-surface relative humidity observations. *Sci. Adv.* **9**, eade6253 (2023).
60. Zhao, L. et al. Global multi-model projections of local urban climates. *Nat. Clim. Change* **11**, 152–157 (2021).
61. Oleson, K. W. & Feddema, J. Parameterization and surface data improvements and new capabilities for the Community Land Model Urban (CLMU). *J. Adv. Model. Earth System.* https://doi.org/10.1029/2018MS001586 (2020).
62. Cheng, Y. et al. U-Surf: a global 1 km spatially continuous urban surface property dataset for kilometer-scale urban-resolving Earth system modeling. *Earth Syst. Sci. Data* **17**, 2147–2174 (2025).
63. Jackson, T. L., Feddema, J. J., Oleson, K. W., Bonan, G. B. & Bauer, J. T. Parameterization of urban characteristics for global climate modeling. *Ann. Assoc. Am. Geogr.* **100**, 848–865 (2010).
64. Arundel, A. V., Sterling, E. M., Biggin, J. H. & Sterling, T. D. Indirect health effects of relative humidity in indoor environments. *Environ. Health Perspect.* **65**, 351–361 (1986).
65. Baughman, A. & Arens, E. A. Indoor humidity and human health–part I: literature review of health effects of humidity-influenced indoor pollutants. *ASHRAE Trans.* **102**, 193–211 (1996).
66. Wolkoff, P. Indoor air humidity, air quality, and health—an overview. *Int. J. Hyg. Environ. Health* **221**, 376–390 (2018).
67. *ANSI/ASHRAE Standard 62.1-2022: Ventilation for Acceptable Indoor Air Quality* (ASHRAE, 2022).
68. *ANSI/ASHRAE Standard 62.1-2013: Ventilation for Acceptable Indoor Air Quality* (ASHRAE, 2013).
69. Salamanca, F., Krpo, A., Martilli, A. & Clappier, A. A new building energy model coupled with an urban canopy parameterization for urban climate simulations—part I. Formulation, verification, and sensitivity analysis of the model. *Theor. Appl. Climatol.* **99**, 331 (2009).
70. Zhang, H. & Yoshino, H. Analysis of indoor humidity environment in Chinese residential buildings. *Build. Environ.* **45**, 2132–2140 (2010).
71. Bueno, B., Pigeon, G., Norford, L. K., Zibouche, K. & Marchadier, C. Development and evaluation of a building energy model integrated in the TEB scheme. *Geosci. Model Dev.* **5**, 433–448 (2012).
72. Guan, H. et al. Response of office building electricity consumption to urban weather in Adelaide, South Australia. *Urban Clim.* **10**, 42–55 (2014).
73. Oleson, K., Bonan, G., Feddema, J., Vertenstein, M. & Kluzek, E. *Technical Description of an Urban Parameterization for the Community Land Model (CLMU)* (NSF National Center for Atmospheric Research, 2010).
74. Lawrence, D. M. et al. The Community Land Model Version 5: description of new features, benchmarking, and impact of forcing uncertainty. *J. Adv. Model. Earth Syst.* **11**, 4245–4287 (2019).
75. Varquez, A. C. G., Kiyomoto, S., Khanh, D. N. & Kanda, M. Global 1-km present and future hourly anthropogenic heat flux. *Sci. Data* **8**, 64 (2021).
76. Li, X. et al. Data for 'Divergent humidity-driven growth in urban air-conditioning energy demand under climate change'. *Zenodo* https://doi.org/10.5281/zenodo.20563953 (2026).

Acknowledgements

We acknowledge the high-performance computing support from the Derecho system (https://doi.org/10.5065/qx9a-pg09) provided by the US NSF National Center for Atmospheric Research (NCAR), sponsored by the US National Science Foundation, for all simulations and analyses conducted in this work.

Author contributions

X.L. and L.Z. conceptualized and designed the research. X.L. developed the dehumidification modeling scheme and performed the simulations and data analyses with suggestions from L.Z., K.O. and Z.L. K.O. performed the analysis on the impact of condensed water on river runoff (Supplementary Table 2). Y.C. provided surface data for the simulations. A.C.G.V. and M.S. provided source data on AHF for model validation. X.L. performed model validation. X.L. drafted the paper. All authors provided comments, suggestions and edits.

Funding

X.L. acknowledges the Laboratory Directed Research and Development Program at Pacific Northwest National Laboratory, a multiprogram national laboratory operated by Battelle for the US Department of Energy (DOE). X.L. is grateful for the support of the Linus Pauling Distinguished Postdoctoral Fellowship program and Proposal Scope 85575 for the research and publication of this work. L.Z., X.L. and Y.C. acknowledge the support by the US National Science Foundation (NSF) (CAREER Award Grant 2145362). X.L., L.Z., Z.L. and X.X. acknowledge the support from Cardiff-University of Illinois System Joint Seed Fund. L.Z. and Y.C. acknowledge the support by the US National Aeronautics and Space Administration (NASA) through a joint Land Cover Land Use Change (LCLUC) and Advanced Modeling Technology (AMT) grant (no. 80NSSC25K7322). K.O. acknowledges funding from the NSF National Center for Atmospheric Research, which is a major facility sponsored by the US National Science Foundation under Cooperative Agreement No. 1852977. A.C.G.V. and M.S. acknowledge the support of JSPS KAKENHI (grant nos. JP21H04573, JP21K14249 and JP23H03599).

Competing interests

The authors declare no competing interests.

Additional information

Extended data is available for this paper at https://doi.org/10.1038/s44284-026-00474-4.

Supplementary information The online version contains supplementary material available at https://doi.org/10.1038/s44284-026-00474-4.

Correspondence and requests for materials should be addressed to Xinchang 'Cathy' Li or Lei Zhao.

Peer review information *Nature Cities* thanks Tianzhen Hong, Mathew Lipson and Chenghao Wang for their contribution to the peer review of this work.

https://doi.org/10.1038/s44284-026-00474-4

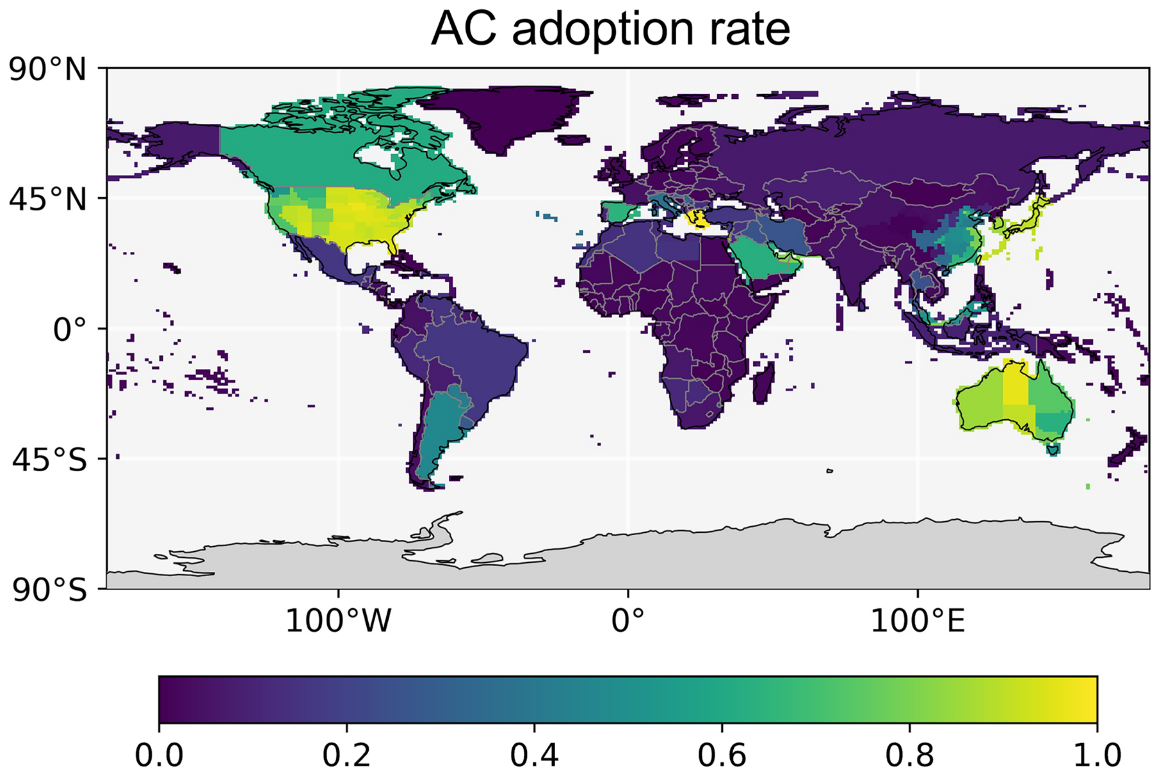

Extended Data Fig. 1 | The air-conditioning (AC) adoption rate used in model simulation. The dataset is described in ref. 41. Basemap from Natural Earth (https://www.naturalearthdata.com/).

https://doi.org/10.1038/s44284-026-00474-4

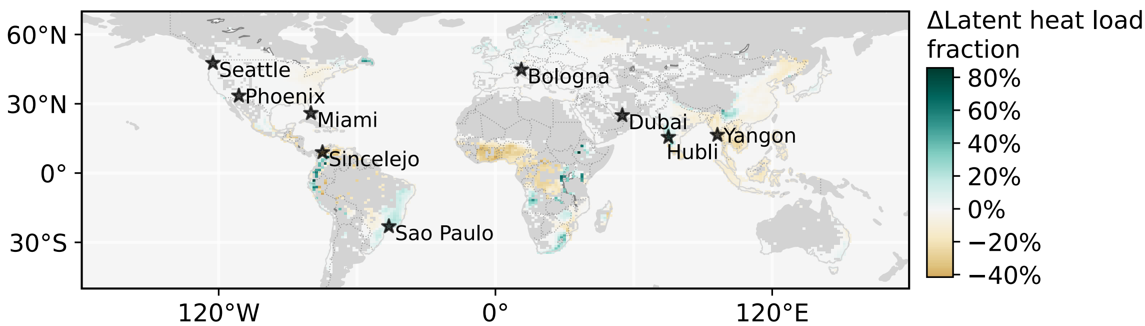

Extended Data Fig. 2 | Locations of selected cities discussed in the study. It is plotted over change in latent heat load fractions as shown in Fig. 1f. Basemap from Natural Earth (https://www.naturalearthdata.com/).

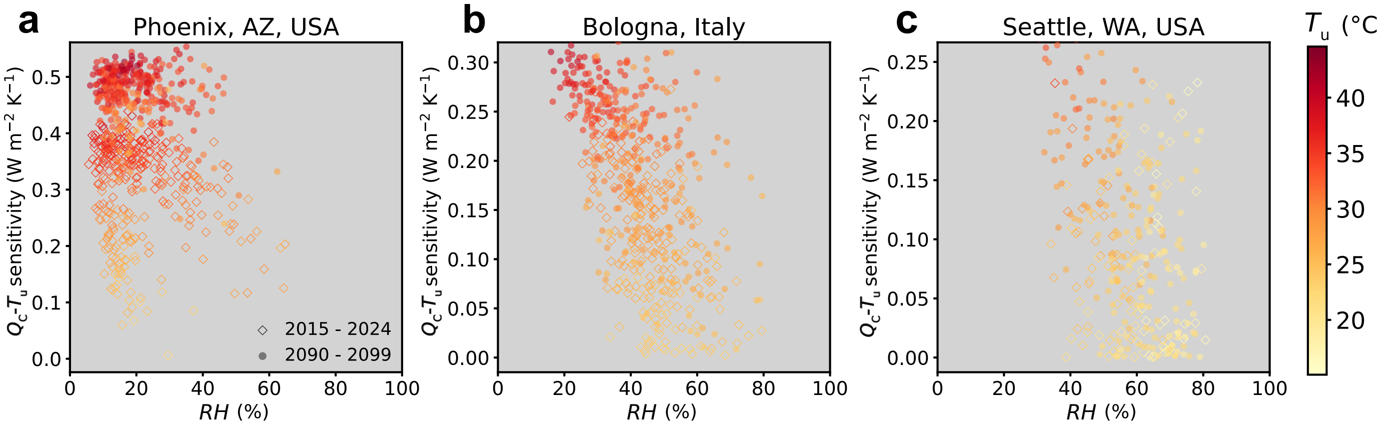

Extended Data Fig. 3 | Relationship between AC energy-temperature (Q-T) sensitivity and RH. Relationship between AC energy-temperature (Q_C-T_u) sensitivity and RH. As in Fig. 3 but for three different cities, Phoenix (a), Bologna (b), and Seattle (c), which exhibit different behaviors in Q_c-T_u sensitivity.

https://doi.org/10.1038/s44284-026-00474-4

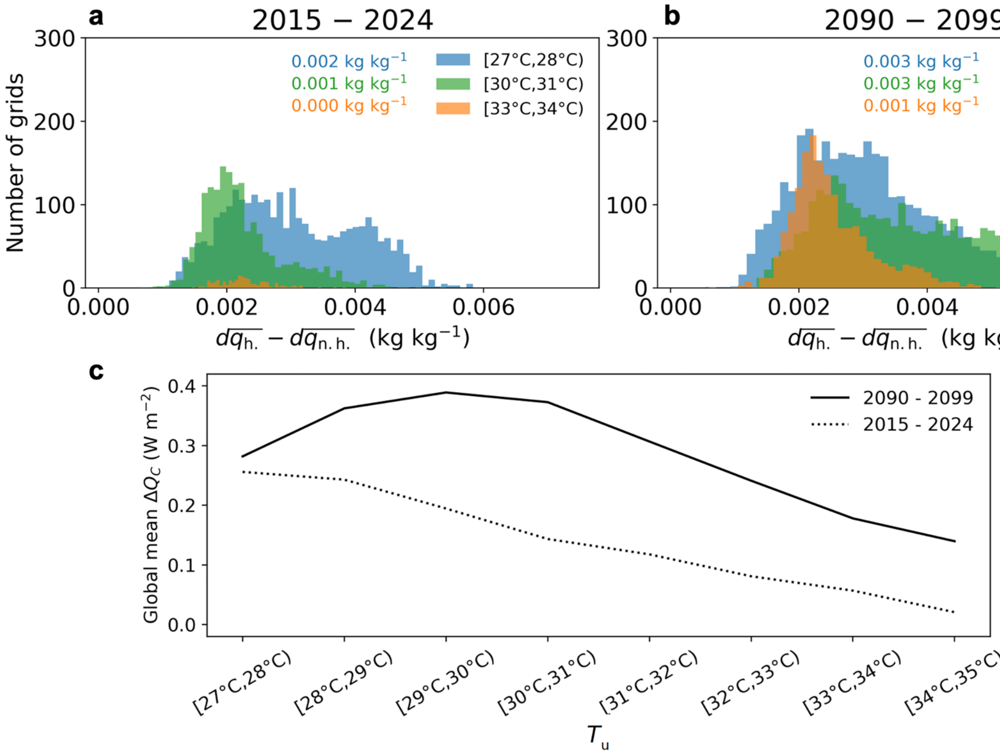

Extended Data Fig. 4 | Changes in excess water content partially explains the trends in global mean differences in AC energy demand (ΔQ_C) between humid and non-humid days. a, **b**, distributions of mean differences in excess water content (amount of moisture that needs to be removed to satisfy RH setpoint) on humid days ($\overline{dq_{h.}}$) and on non-humid days ($\overline{dq_{n.h.}}$) for three temperature bins, for 2015 – 2024 (**a**) and 2090 – 2099 (**b**). Annotations inside **a** and **b** denote the area-weighted global averages for the three temperature bins. **c**, trends in global mean ΔQ_C between humid and non-humid days for integer urban air temperature (T_u) bins from 27 to 35 °C.

 https://doi.org/10.1038/s44284-026-00474-4

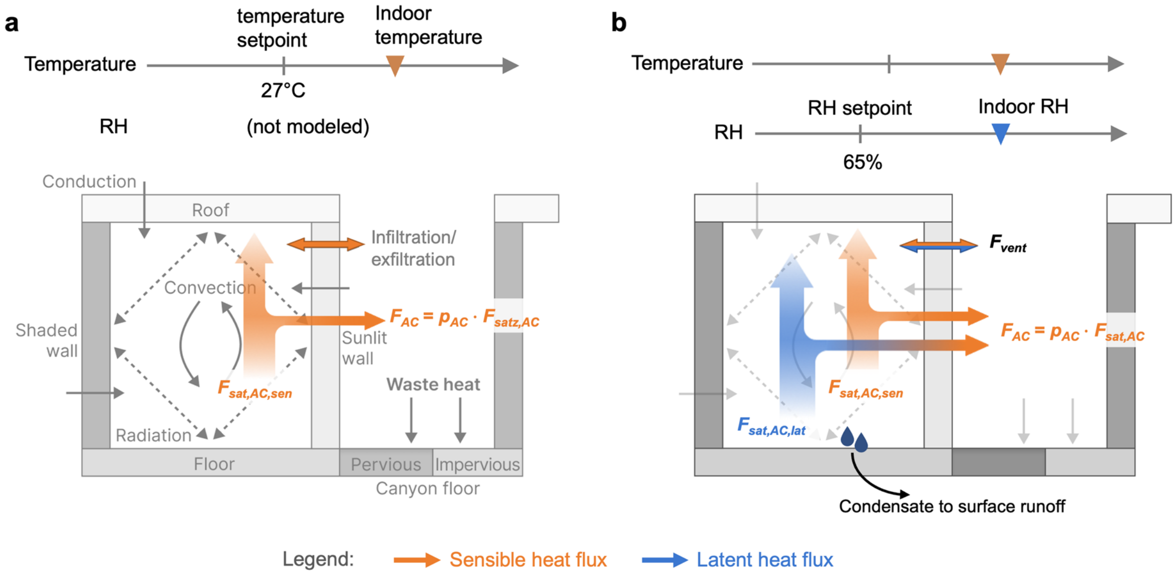

Extended Data Fig. 5 | Schematic diagram of the new scheme for latent heat load and dehumidification energy demand modeling on an illustrative hot and humid day. a, AC energy demand modeling under the explicit AC adoption scheme[41], which provides the basis for the model development of this study. **b**, AC energy demand modeling enhanced with latent heat load by this study. *RH*, relative humidity. F_{vent}, energy flux due to infiltration/exfiltration. F_{AC}, AC energy demand flux. p_{AC}, AC adoption rate. $F_{sat,AC}$, AC energy demand flux under 100% (saturated) AC adoption. $F_{sat,AC,lat}$, latent heat load (dehumidification energy demand) flux. $F_{sat,AC,sen}$, sensible heat load (cooling energy demand) flux.

https://doi.org/10.1038/s44284-026-00474-4

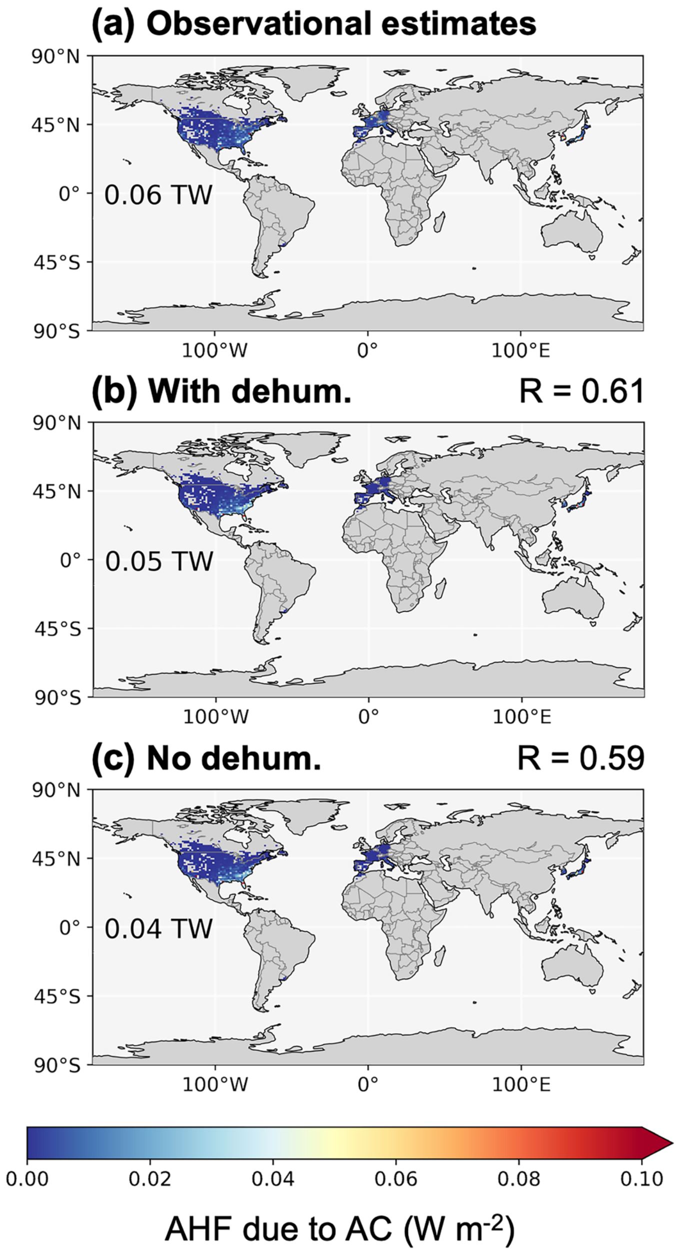

Extended Data Fig. 6 | Good agreements in modeled anthropogenic heat flux (AHF) due to AC for available countries/regions in 2010 – 2014. (**a**) observational estimates derived from an updated data based on ref. 75 and other observational data products (see Supplementary Note 5), (**b**) simulated AHF due to AC using the new scheme in this study where dehumidification is modeled ("With dehum."), and (**c**) simulated AHF due to AC using the default CLMU scheme without dehumidification ("No dehum."). Numbers annotated on the left side in subpanels represent the total anthropogenic heat (in terawatts) plotted in each panel. R is the pattern correlation between each panel and panel (**a**). Basemap in **a**–**c** from Natural Earth (https://www.naturalearthdata.com/).

 https://doi.org/10.1038/s44284-026-00474-4

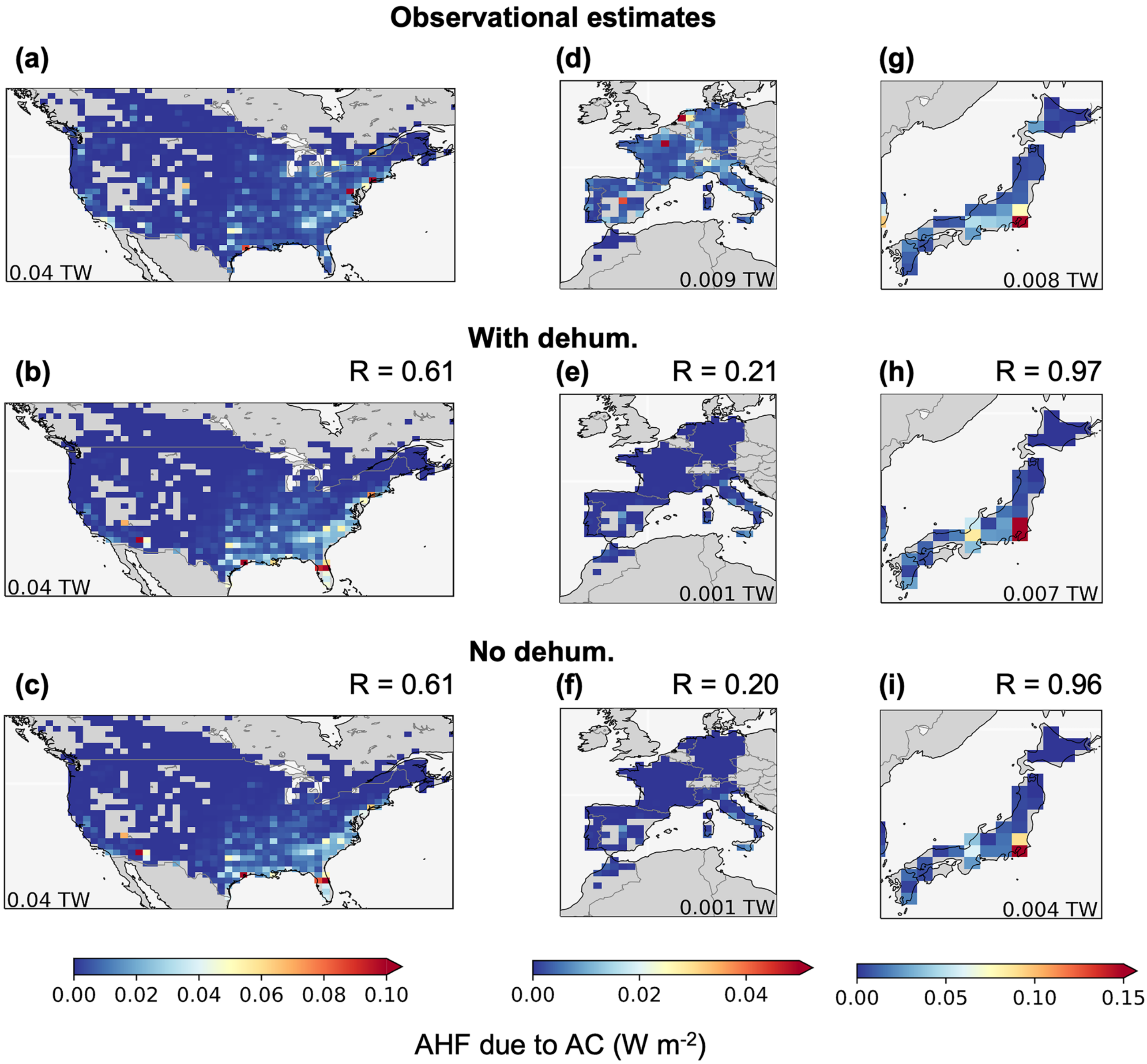

Extended Data Fig. 7 | As in Extended Data Fig. 6 but for the zoomed-in views of three regions. (**a**-**c**) Contiguous US and parts of Canada, (**d**-**f**) parts of Europe and North Africa, and (**g**-**i**) Japan. Observational estimates are provided in the first row (**a, d, g**), simulated results using the scheme in this study in the middle row (**b, e, h**), and simulated results using the default scheme in the bottom row (**c, f, i**). Panels in a column share the same colorbar at the bottom of each column. Basemap in **a**–**i** from Natural Earth (https://www.naturalearthdata.com/).

https://doi.org/10.1038/s44284-026-00474-4

Extended Data Table 1 | Humidity effect on building energy demand varies substantially in local-scale studies

Paper	Study region	Study period	Building type	Methods	Data	Relevant findings
Ref.[16]	12 cities in different climate zones of China	1961 - 2017	Typical office building	Mathematical model for design load calculations from the design code for HVAC of civil buildings (GB50736-2012)	* Thermal properties and Indoor design parameters from GB50736-2012 * Meteorological data from downtown weather stations	RH decreases by 1 - 9%, leading to a 1 - 8% decrease in dehumidification load.
Ref.[17]	Tianjin, China	2009 - 2020	A 22-story office building with a total area of 12,552 m2 and total height of 98m	TRNSYS simulations	* Design parameters from Design Standard for Energy Efficiency in public buildings (GB50189-2005) & local design/energy codes * Meteorological data from urban and rural weather stations	During cooling season, urban RH is lower than rural RH by 5 - 12%, which leads to the latent heat load of the urban building being 49 % - 68 % lower than the rural building.
Ref.[20]	4 USA cities in different climate zones	- (TMY)	3 building types (school, office, apartment)	DOE benchmark models (EnergyPlus)	* Design parameters from DOE commercial building benchmark models * Weather files based on Typical Meteorological Years (TMYs)	Miami: increasing RH from 73% to 88% increases energy use intensity (EUI) by 4 to 5%; Ann Arbor: increasing RH from 75% to 86% increases EUI by 1%.
Ref.[21]	801 locations in different climate zones of the USA	- (TMY)	ASHRAE Standard 90.1–2016 medium office prototypes	EnergyPlus	* Weather files based on TMY3 from EnergyPlus weather data online	For the same building in the same ASHRAE climate zone, source energy consumption in moist climate subtype is up to 47% higher than in marine climate subtype (i.e., drier climate).
Ref.[18]	Hong Kong, China	2004 - 2013	A typical hypothetic 30-story residential building	DeST simulations	Weather files from urban and rural weather stations	Average urban nighttime specific humidity is higher than the rural counterpart by 0.1 to 0.7 g/kg. This leads to higher latent cooling load in the urban building than rural building by 47% to 96%.
Ref.[19]	Milan, Italy	2002 - 2008	A typical residential building, representative of the 1961–1975 housing stock in Milan (a stand-alone ten-story tower)	WUFI Plus 3.0.3	* Properties & design parameters based on local regulations and design standards * Weather files from an urban-rural station pair	Urban specific humidity is lower than the rural counterpart by 0.27 to 1.44 g/kg, which leads to 74–78% lower dehumidification loads

 https://doi.org/10.1038/s44284-026-00474-4

Extended Data Table 2 | The latent heat load fractions modeled in this study agree well with local case studies

Paper	Location	Methods	Reported Estimates	Our results (mean)	Our results (median)	Source of reported estimates
Ref.[42]	Houston, USA	EnergyPlus simulations	11%	16%	13%	Fig. 5 and 6
Ref.[43]	Beijing, China	TRNSYS simulations	22%	21%	8%	Sect. 3.2.1
	Shanghai, China		27%	27%	21%	Sect. 3.2.2
Ref.[44]	Guangzhou, China	Mathematical model	33%	39%	39%	Table 3; Fig. 10
	Wuhan, China		36%	36%	37%	
	Jiuquan, China		0%	0%	0%	
Ref.[18]	Hong Kong, China	DeST simulations	26 – 34%	42%	40%	Sect. 3.2.2
Ref.[17]	Tianjin, China	TRNSYS simulations	17%	15%	3%	Sect. 3.2
Ref.[19]	Milan, Italy	WUFI Plus 3.0.3 simulations	4 – 6%	3%	0%	Fig. 4b & 4c

Both reported and our estimates are for summer (around June, July, and August). Green indicates our estimates are within ±15% of reported values/ranges in the literature.

nature portfolio

Corresponding author(s): Xinchang "Cathy" Li, Lei Zhao

Last updated by author(s): Jun 5, 2026

Reporting Summary

Nature Portfolio wishes to improve the reproducibility of the work that we publish. This form provides structure for consistency and transparency in reporting. For further information on Nature Portfolio policies, see our Editorial Policies and the Editorial Policy Checklist.

Statistics

For all statistical analyses, confirm that the following items are present in the figure legend, table legend, main text, or Methods section.

n/a	Confirmed	
☐	☒	The exact sample size (n) for each experimental group/condition, given as a discrete number and unit of measurement
☒	☐	A statement on whether measurements were taken from distinct samples or whether the same sample was measured repeatedly
☒	☐	The statistical test(s) used AND whether they are one- or two-sided *Only common tests should be described solely by name; describe more complex techniques in the Methods section.*
☒	☐	A description of all covariates tested
☒	☐	A description of any assumptions or corrections, such as tests of normality and adjustment for multiple comparisons
☐	☒	A full description of the statistical parameters including central tendency (e.g. means) or other basic estimates (e.g. regression coefficient) AND variation (e.g. standard deviation) or associated estimates of uncertainty (e.g. confidence intervals)
☒	☐	For null hypothesis testing, the test statistic (e.g. F, t, r) with confidence intervals, effect sizes, degrees of freedom and P value noted *Give P values as exact values whenever suitable.*
☒	☐	For Bayesian analysis, information on the choice of priors and Markov chain Monte Carlo settings
☒	☐	For hierarchical and complex designs, identification of the appropriate level for tests and full reporting of outcomes
☒	☐	Estimates of effect sizes (e.g. Cohen's d, Pearson's r), indicating how they were calculated

Our web collection on statistics for biologists contains articles on many of the points above.

Software and code

Policy information about availability of computer code

Data collection	Data were generated through simulations using open-source, custom modified version of the Community Earth Systems Model (CESM). The code is available here: https://github.com/cathyxinchangli/CTSM/tree/dehumidification.
Data analysis	Data analysis was conducted using Python on U.S. NSF NCAR's supercomputer Derecho.

For manuscripts utilizing custom algorithms or software that are central to the research but not yet described in published literature, software must be made available to editors and reviewers. We strongly encourage code deposition in a community repository (e.g. GitHub). See the Nature Portfolio guidelines for submitting code & software for further information.

Data

Policy information about availability of data

All manuscripts must include a data availability statement. This statement should provide the following information, where applicable:

- Accession codes, unique identifiers, or web links for publicly available datasets
- A description of any restrictions on data availability
- For clinical datasets or third party data, please ensure that the statement adheres to our policy

The CESM simulation results that support the findings of this study are archived and publicly available in the Zenodo repository: https://doi.org/10.5281/zenodo.20563953. The base maps are available from https://www.naturalearthdata.com/. Source data are provided with this paper.

Research involving human participants, their data, or biological material

Policy information about studies with human participants or human data. See also policy information about sex, gender (identity/presentation), and sexual orientation and race, ethnicity and racism.

Reporting on sex and gender	N/A
Reporting on race, ethnicity, or other socially relevant groupings	N/A
Population characteristics	N/A
Recruitment	N/A
Ethics oversight	N/A

Note that full information on the approval of the study protocol must also be provided in the manuscript.

Field-specific reporting

Please select the one below that is the best fit for your research. If you are not sure, read the appropriate sections before making your selection.

☐ Life sciences ☐ Behavioural & social sciences ☒ Ecological, evolutionary & environmental sciences

For a reference copy of the document with all sections, see nature.com/documents/nr-reporting-summary-flat.pdf

Ecological, evolutionary & environmental sciences study design

All studies must disclose on these points even when the disclosure is negative.

Study description	We develop a new physics-based parameterization scheme to model indoor humidity and dehumidification energy demand in the urban building energy model of the Community Earth System Model (CESM). The scheme adopts a setpoint approach and simulates both the sensible (for cooling) and latent (for dehumidification) AC energy demand required to maintain indoor comfort and health. We validate the scheme both on its ability to simulate total AC energy demand globally and on its performance simulating the relative contribution of sensible and latent heat load at the local scale. We conduct a global simulation driven by atmospheric forcings from a fully-coupled simulation under a high emission scenario, keeping socioeconomic factors such as AC adoption rate and urban extent at the present-day level to isolate climate change effects. Daily average values of urban air temperature (Tu), relative humidity (RH), specific humidity (q), and sensible and latent heat load fluxes of AC energy demand for the first decade (2015 – 2024) and the last decade (2090 – 2099) of the simulation period are analyzed.
Research sample	N/A
Sampling strategy	N/A
Data collection	Data are automatically saved to computer storage as the simulations are being run.
Timing and spatial scale	The simulations are run at 30-min time steps and 0.9375° latitude × 1.25° longitude spatial resolution, over all urban land areas globally. Data are averaged over each day and saved at daily frequencies.
Data exclusions	N/A
Reproducibility	The updated CESM code used for simulation is publicly available on GitHub at https://github.com/cathyxinchangli/CTSM/tree/dehumidification. Results from CESM simulations are publicly available at https://doi.org/10.5281/zenodo.20563953. Source data for each Figure, Extended Data Figure, and Supplementary Figure are provided with the study
Randomization	N/A
Blinding	N/A

Did the study involve field work? ☐ Yes ☒ No

Reporting for specific materials, systems and methods

We require information from authors about some types of materials, experimental systems and methods used in many studies. Here, indicate whether each material, system or method listed is relevant to your study. If you are not sure if a list item applies to your research, read the appropriate section before selecting a response.

Materials & experimental systems

n/a	Involved in the study
☒	☐ Antibodies
☒	☐ Eukaryotic cell lines
☒	☐ Palaeontology and archaeology
☒	☐ Animals and other organisms
☒	☐ Clinical data
☒	☐ Dual use research of concern
☒	☐ Plants

Methods

n/a	Involved in the study
☒	☐ ChIP-seq
☒	☐ Flow cytometry
☒	☐ MRI-based neuroimaging

Plants

Seed stocks	N/A
Novel plant genotypes	N/A
Authentication	N/A